https://doi.org/10.5194/egusphere-2022-1
Preprint. Discussion started: 14 March 2022

Indices of Extremes: Geographic patterns of change in extremes and associated vegetation impacts under climate intervention

Mari R. Tye[1], Katherine Dagon[1], Maria J. Molina[1], Jadwiga H. Richter[1], Daniele Visioni[2], Ben Kravitz[3,4], Claudia Tebaldi[5], Simone Tilmes[6]

[1] Climate Global Dynamics Laboratory, National Center for Atmospheric Research, Boulder, CO
[2] Sibley School for Mechanical and Aerospace Engineering, Cornell University, Ithaca, NY
[3] Department of Earth and Atmospheric Sciences, Indiana University, Bloomington, IN
[4] Atmospheric Sciences and Global Change Division, Pacific Northwest National Laboratory, Richland, WA
[5] Lawrence Berkeley National Laboratory, Berkeley, CA
[6] Atmospheric Chemistry, Observations, and Modeling Laboratory, National Center for Atmospheric Research, Boulder, CO

Correspondence to: Mari R. Tye (maritye@ucar.edu)

Abstract Extreme weather events have been demonstrated to be increasing in frequency and intensity across the globe and are anticipated to increase further with projected changes in climate. Solar climate intervention strategies, specifically stratospheric aerosol injections (SAI), have the potential to minimize some of the impacts of a changing climate while more robust reductions in greenhouse gas emissions take effect. However, to date little attention has been paid to the possible responses of extreme weather and climate events under climate intervention scenarios. We present an analysis of 16 extreme surface temperature and precipitation indices, and associated vegetation responses, applied to the Geoengineering Large Ensemble (GLENS). GLENS is an ensemble of simulations performed with the Community Earth System Model (CESM1) where SAI is simulated to offset the warming produced by a high emission scenario throughout the 21st century, maintaining surface temperatures at 2020 levels.

GLENS is generally successful at maintaining global mean temperature near 2020 levels, however it does not completely offset some of the projected warming in northern latitudes. Some regions are also projected to cool substantially in comparison to the present day, with the greatest decreases in daytime temperatures. The differential warming/cooling also translates to fewer very hot days but more very hot nights during the summer, and fewer very cold days or nights compared to the current day. Extreme precipitation patterns, for the most part, are projected to reduce in intensity in areas that are wet in the current climate and increase in intensity in dry areas. We also find that the distribution of daily precipitation becomes more consistent with more days with light rain, and fewer very intense events than occur currently. In many regions there is a reduction in the persistence of long dry and wet spells compared to present day. However, asymmetry in the night and day temperatures, together with changes in cloud cover and vegetative responses could exacerbate drying in regions that are already sensitive to

https://doi.org/10.5194/egusphere-2022-1
Preprint. Discussion started: 14 March 2022

drought. Overall, our results suggest that while SAI may ameliorate some of the extreme weather hazards produced by global warming, it would also present some significant differences in the distribution of climate extremes compared to the present day.

Short Summary We examined the potential effect of stratospheric aerosol injections (SAI) on extreme temperature and precipitation. SAI may cause daytime temperatures to cool but nighttime to warm. Daytime cooling may occur in all seasons across the globe, with largest decreases in the summer. In contrast, nighttime warming may be greatest at high latitudes in the winter. SAI may reduce the frequency and intensity of extreme rainfall. The combined changes may exacerbate drying over parts of the global South.

1 Introduction

The impacts of extreme events are, and will increasingly be, disproportionately experienced by the most vulnerable populations and ecosystems (Stott, 2016). Furthermore, the observed increases in frequency and severity of extreme weather events will worsen with projected changes in climate, and will likely change more rapidly than the underlying climate base state (Seneviratne et al., 2021). Solar climate intervention strategies, specifically stratospheric aerosol injections (SAI) have been identified as a potential mechanism by which the most extreme effects resulting from climate change might be moderated while other more long-term strategies (namely cutting greenhouse gas emissions and eventually direct reduction of the volume of CO_2 in the atmosphere) take effect. However, to understand whether SAI is a viable solution requires a full understanding of different Earth system responses and their relative impacts in different locations. In particular, the responses of the extreme weather and climate events and the attendant impacts on issues such as food and water security, health and livelihoods have had insufficient attention to date. Noting that a risk-risk assessment (Florin, 2021) of the potential consequences of SAI needs to be informed by transdisciplinary research and accommodate a reflection of the human and ecological responses to climate change and mitigation activities (Carlson & Trisos, 2018), here we study the effects of SAI on the hazard component of the risk. That is, our attention is focused exclusively on the effects of SAI on the physical climate system.

The potential of SAI to depress temperatures is premised on the tendency of aerosol emissions from natural causes such as volcanic eruptions or mega-fires to reflect shortwave radiation and cool the planet (Budyko, 1977). However, the sustained influence of SAI may be considerably different from the temporary effects from a volcanic eruption (Duan et al., 2019). Furthermore, it is unlikely that any intervention will return the climate to a pre-

https://doi.org/10.5194/egusphere-2022-1
Preprint. Discussion started: 14 March 2022

industrial state (Kravitz et al., 2021), but there will be trade-offs to manage as many different climatic variables that will be affected by alternative design targets (Lee et al., 2020). It is widely acknowledged that the Earth system responses to SAI will vary temporally and spatially (Cheng et al., 2019; Simpson et al., 2019) as well as in response to the injection location (MacMartin et al., 2018; Kravitz et al., 2019). Responses in the hydrological cycle are complicated by intra- to inter-annual changes in the location of the Inter Tropical Convergence Zone (Haywood et al., 2013) and conflicting signals in atmospheric-oceanic teleconnections such as ENSO (Gabriel and Robock, 2015; Malik et al., 2020), in addition to energetic constraints (Allen and Ingram, 2002; Ingram, 2016). Furthermore, the spatial and temporal distribution of extreme precipitation has become more skewed in response to temperature increases, such that the most extreme events may not have as linear a correlative relationship with Clausius-Clapeyron as previously assumed (Guerreiro et al., 2018; Pendergrass and Knutti, 2018; Allan et al., 2020). Thus, it is essential to explore how extreme temperature and precipitation may respond to manufactured changes in atmospheric aerosols.

A number of studies have examined the influence of SAI on different extreme events, finding that the cumulative effects of changes in humidity and temperature affect many aspects of the hydrometeorological cycle from Sahelian greening (Da-Allada et al., 2020; Pinto et al., 2020), streamflow responses (Wei et al., 2018), extreme heatwaves (Dagon and Schrag, 2017), and the location and intensity of tropical and extratropical cyclones (Tilmes et al., 2020, Gertler et al., 2020; Irvine et al., 2019). Cheng et al. (2019)'s assessment that decreases in global mean soil moisture and mean precipitation are not spatially consistent, highlight the spatial and temporal variability in precipitation and the need to examine more than just the annual mean and most extreme events. Furthermore, changes in precipitation and temperature extremes due to SAI may have unintended consequences such as impacts on drought duration or severity, vegetation productivity, and terrestrial ecosystems (Dagon and Schrag 2019; Odoulami et al. 2020; Zarnetske et al. 2021). The nuances of these consequences become far more apparent when using models that can specifically simulate the responses from atmospheric aerosols (Visioni et al., 2021). To support informed decision-making, we present an in-depth assessment of the changes in extreme temperature and precipitation using a large model ensemble that simulates the responses from aerosols and enables an assessment of the internal variability.

The World Climate Research Program's Expert Team on Climate Change Detection and Indices (ETCCDI; Klein Tank et al., 2009; Zhang et al, 2011) developed a core set of indicators for use with daily temperature and precipitation extremes. These facilitate comparison across spatial and temporal scales, as well as across different model and observation platforms, and have been widely used with observations and climate projections (e.g.

https://doi.org/10.5194/egusphere-2022-1
Preprint. Discussion started: 14 March 2022

Alexander et al., 2020; Donat et al., 2020; Tebaldi et al., 2021; Tye et al., 2021) and to a lesser extent climate intervention studies (Ji et al., 2018; Aswathy et al., 2015; Curry et al., 2014; Muthyala et al., 2018 a, b). We present an analysis of the indices applied to the Geoengineering Large Ensemble (GLENS; Tilmes et al., 2018). GLENS was performed using the NCAR Community Earth System Model v1, with the Whole Atmosphere Community Climate Model as its atmospheric component (CESM1(WACCM)). CESM1 uses the Community Land Model, version 4.5 (CLM4.5) as its land model component. CLM4.5 includes active terrestrial carbon and nitrogen cycling, including photosynthesis and respiration. While the model uses prescribed distributions of vegetation, there is a prognostic seasonal cycle of leaf area index that can respond to climate changes (Oleson et al. 2013). The GLENS dataset consists of simulations from 2020 to 2100 with and without SAI using the RCP8.5 emissions scenario to drive concentrations of atmospheric CO_2. Hence, it offers a chance to identify where responses to solar climate intervention may be most pronounced, their likely direction of change with respect to the current climate, and where there may be differences, benefits and tradeoffs between a high CO_2 world and a world with high CO_2 and geoengineering.

The performance and projections of the ETCCDI in the Coupled Model Intercomparison Project v.5 (CMIP5), of which CESM1 is one contribution, has been well documented for several emissions scenarios (Sillmann et al., 2013a,b; Tebaldi and Wehner, 2018). Subsets of the ETCCDI have also been examined for both GLENS (Pinto et al., 2020) and GeoMIP simulations (Aswarthy et al., 2015; Curry et al., 2014; Ji et al., 2018; Kuswanto et al., 2021). Although Muthalya et al. (2018 a,b) presented a comprehensive analysis of the temperature and precipitation extreme indices, the simulations adopted a solar dimming approach. Thus, this is the first comprehensive comparison of temperature and precipitation extreme indices responses to SAI using a fully coupled ocean-atmosphere model with temporally varying sulfur dioxide injections. Using the ETCCDI indices, rather than the mean, facilitates a balanced spatial assessment of the likely responses to SAI such as: efficacy in keeping the range of extreme weather events similar to that of the control period climate (2010-2029); performance in mitigating the worst effects of climate change projected under RCP8.5; differential effects in the location and extent of extreme changes in the hydrological cycle.

The article is organized as follows. Section 2 briefly describes the GLENS dataset and presents the temperature and precipitation indices. Section 3 synthesizes the projected changes in extreme indices with respect to the control period climate and the end of century projections without climate intervention. Section 4 links these results to vegetative responses in the light of other similar research and Section 5 concludes.

https://doi.org/10.5194/egusphere-2022-1
Preprint. Discussion started: 14 March 2022

2 Data and methods

2.1 Model Simulations

The analysis utilizes the GLENS dataset (Tilmes et al., 2018) to identify the possible signals of change in extreme temperature and precipitation under a high emissions scenario. GLENS involves sulfur dioxide (SO_2) injections at four locations (30°N, 15°N, 15°S, and 30°S) to offset changes over the period 2020-2100 in global mean temperature (T0), the interhemispheric temperature gradient (T1), and the equator-to-pole temperature gradient (T2) under RCP8.5 (the high emissions Representative Concentration Pathway). The injection amounts at each location are adjusted independently using a feedback algorithm to maintain the three temperature gradients at ~2020 levels (MacMartin et al., 2013, 2017; Kravitz et al., 2016, 2017). By the end of the 21st century, GLENS offsets approximately 5°C of global warming, and injection rates reach over 40 Tg SO_2/year. The details of GLENS are described in more detail by Tilmes et al. (2018) and Kravitz et al. (2017) and are summarized in Table 1.

Table 1: Summary of simulations carried out as part of the GLENS project: simulation name, ensemble members, simulation time period, and analysis period.

Simulation	Ensemble Members	Time Period	Analysis Period
RCP8.5	3 (001-003)	2010-2097	'End of Century' (EC, 2075-2095) and BASE (2010-2030)
RCP8.5	17 (004-020)	2010-2030	BASE (2010-2030)
Geoengineering (GLENS)	20 (001-020)	2020-2099	EC (2075-2095)

The complete GLENS dataset comprises three RCP8.5 simulations without geoengineering from 2010 to 2095 or 2099, and additional 17 members from 2010 to 2030. Hence, there are a total of 20 simulations without geoengineering for a 'control' period of 2010-2030, referred to as BASE. The 20-member SAI intervention simulations are branched from their corresponding BASE member in 2020, and are referred to here as GLENS. Results are presented for the differences between an end of the century (EC) period of 2075-2095, where the differences between GLENS (EC) or RCP8.5 (EC) and RCP8.5 2010-2029 (BASE) are most readily discernible from natural variability.

https://doi.org/10.5194/egusphere-2022-1
Preprint. Discussion started: 14 March 2022

We note that simulations represent geoengineering to moderate the extreme climate changes expected at the end of the century under RCP8.5, with no additional reduction in anthropogenic carbon emissions. While useful for extracting signals in a noisy climate system, deployments of geoengineering are likely to be more moderate and made in combination with other methods of addressing climate change, such as greenhouse gas emission reductions and negative emissions (Tilmes et al., 2020; MacMartin et al., 2018; Keith and Irvine, 2016; Honegger et al., 2021).

2.2 Extreme Indices

A subset of the full set of ETCCDI indices (from hereon referred to as ETCCDI) are listed in Table 2 and discussed in this paper. Given the number of indices and global coverage of the analysis, only the annual ETCCDI are discussed in this paper. However, some seasonality is implicit in indices such as the annual coldest and warmest temperatures.

Table 2: Selection of extreme indices developed by ETCCDI (Klein Tank et al., 2009). Percentiles marked with * were estimated from a base period of 2010-2030 but are not included in the main text; values are calculated as a climatological average for the end of the century (2075-2095). Indices in italics are not included in the main text.

Index	Name	Definition	Unit	Type
TNn	Coldest night	Annual minimum daily minimum temperature	°C	Fixed index
TXn	Coldest day	Annual minimum daily maximum temperature	°C	Fixed index
TNx	Warmest night	Annual maximum daily minimum temperature	°C	Fixed index
TXx	Warmest day	Annual maximum daily maximum temperature	°C	Fixed index
FD	Frost days	Number of days where Tn ≤ 0°C	days	Fixed threshold
ID	Ice days	Number of days where Tx ≤ 0°C	days	Fixed threshold
TR	Tropical nights	Number of days where Tn ≥ 20°C	days	Fixed threshold
SU	Summer days	Number of days where Tx ≥ 25°C	days	Fixed threshold
Tn10	*Cool nights*	*Number of days per year when the daily minimum temperature (Tn) is <10th percentile**	*days*	*Percentile based threshold*
Tx10	*Cool days*	*Number of days per year where the daily maximum temperature (Tx) is <10th percentile**	*days*	*Percentile based threshold*
Tn90	*Warm nights*	*Number of days when Tn >90th percentile**	*days*	*Percentile based threshold*

https://doi.org/10.5194/egusphere-2022-1
Preprint. Discussion started: 14 March 2022

Index	Name	Definition	Unit	Type
Tx90	*Warm days*	*Number of days when Tx >90th percentile**	*days*	*Percentile based threshold*
PRCPTOT	Total Rainfall	Annual sum of precipitation (PR)	mm	Fixed index
SDII	Simple Daily Intensity	Mean precipitation falling on days where PR ≥ 1mm	mm	Fixed index
Rx1day	Wettest Day	Annual maximum precipitation in a single day	mm	Fixed index
Rx5day	Wettest Pentad	Annual maximum precipitation falling on 5 consecutive days	mm	Fixed index/ Spell
CDD	Consecutive dry days	Longest spell of consecutive days where PR ≤ 1mm	days	Fixed index/ Spell
CWD	Consecutive wet days	Longest spell of consecutive days where PR ≥ 1mm	days	Fixed index
R10mm	Heavy precipitation days	Number of days when precipitation ≥10mm	days	Fixed threshold
R20mm	Very heavy precipitation days	Number of days when precipitation ≥20mm	days	Fixed threshold
R95PTot	*Very wet days*	*Total precipitation from days >95th percentile**	*mm*	*Percentile based threshold*
R99PTot	*Extremely wet days*	*Total precipitation from days >99th percentile**	*mm*	*Percentile based threshold*

The ETCCDI fall into three groups: *Fixed Indices* such as the annual minima and maxima and spell duration; *Fixed Thresholds* such as the annual frequency of days with >10mm precipitation; and *Percentile Thresholds* such as the annual frequency of days with temperatures exceeding the 90th percentile. Fixed threshold indices are useful where they give a sense of the implications of changed temperatures and precipitation patterns. For instance, the number of days above zero may indicate the potential for vegetation growth. However, fixed threshold indices can be meaningless where they seldom occur and will not change (such as the number of days falling below 0°C in the Arabian Peninsula). The duration of longest consecutive dry periods (CDD), or dry spells, serve as a simple proxy for drought conditions. Both CDD and the longest consecutive number of wet days (CWD) are calculated as the longest period in any given year in the 20-year analysis period with consecutive days of precipitation above

https://doi.org/10.5194/egusphere-2022-1
Preprint. Discussion started: 14 March 2022

or below 1mm. In contrast with Silmann et al. (2013 a, b) we did not allow the spell duration to extend beyond a year.

Changes in fixed threshold ETCCDI can be critical indicators for health and environmental impacts (Mearns et al., 1984; Mitchell et al., 2016), and tend to change more rapidly than changes in the mean (Meehl et al., 2000; Asadieh and Krakauer, 2015). While such indices are not always "extreme" in and of themselves, they have been demonstrated to be more sensitive to change (e.g. Alexander et al., 2006; Frich et al., 2002). Percentile based ETCCDI, including the frequency of cold/warm days and nights (TX10/TX90, TN10/TN90) and proportional contribution of the heaviest events to the annual total precipitation (R95pTot, R99pTot), demonstrated very similar patterns to those of other ETCCDI. For completeness they are referenced in Table 2, but for brevity the ETCCDI that are in italic font have not been shown in the main text.

To facilitate comparison with other analyses using the GLENS dataset (e.g. Simpson et al., 2019) and to provide the greatest signal-to-noise ratio, we present absolute difference anomalies in ETCCDI between an end of the century period (2075-2095; EC) for simulations with and without SO_2 injections (GLENS and RCP 8.5, respectively) and the BASE (2010-2030). Regional means are calculated over the 46 land-only Reference Regions produced for Assessment Report 6 (Iturbide et al., 2020) and illustrated in Figure 1. We caution that using a control period of 2010-2030 prevents direct comparison with other projections of ETCCDI from the CMIP5 archive (e.g. Sillmann et al. 2013b; Diffenbaugh and Giorgi, 2012).

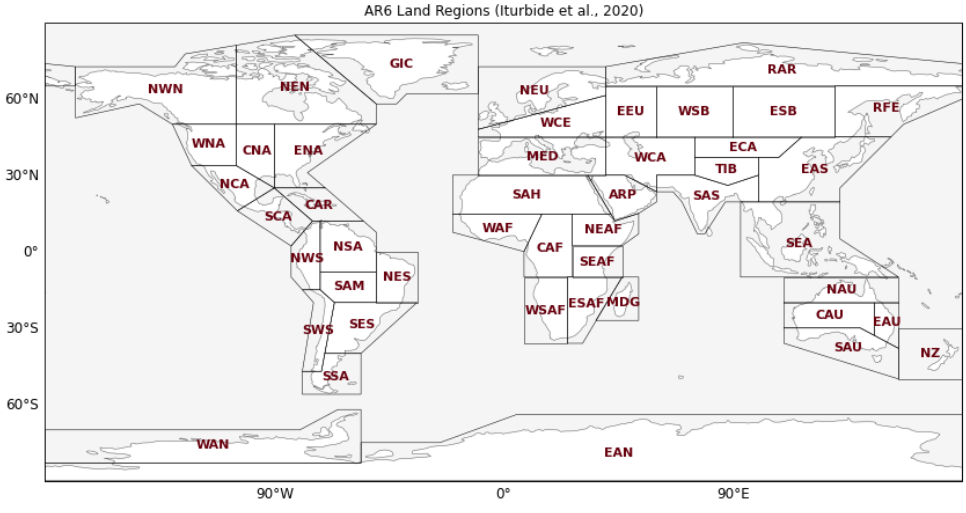

Figure 1: AR6 Reference Regions for Land (Source: Iturbide et al., 2020)

https://doi.org/10.5194/egusphere-2022-1
Preprint. Discussion started: 14 March 2022

Changes in precipitation patterns over land, and associated changes in soil moisture, are intrinsically linked to vegetation through processes like evapotranspiration, water consumption and albedo effects (Cheng et al., 2019). Some of the ETCCDI in Table 2 are more intuitively linked to vegetation responses than others. For instance, CDD and CWD are associated with droughts, FD and ID can be connected to growing potential, and TN90 and TX90 have important implications for heatwaves. Furthermore, the processes linking precipitation and temperature with impacts on vegetation are influenced by increasing atmospheric CO_2 which tends to increase vegetation productivity and decrease evapotranspiration (ET; Dagon and Schrag, 2016) through changes in plant water use efficiency. In addition, the increase in diffuse radiation from SAI could also increase vegetation productivity (Xia et al., 2016). The effects of cloud cover have also been linked to differential rates of change in nighttime or daytime temperatures and the associated vegetative responses in different locations (Cox et al., 2020). These effects are explored further in Section 4.

3 Temperature and Precipitation Response

While we analyzed all of the ETCCDI presented in Table 2, general spatial patterns of change are similar across many of them. A selection of the ETCCDI or regions demonstrating the largest changes are presented in the following text, with additional figures included in the Supplemental Material. The significance of the difference between GLENS EC and BASE, or RCP8.5 and BASE, was assessed using a two-sided Student's *t*-test at the 5% level.

3.1 Temperatures

3.1.1 Fixed Indices

GLENS EC (2075-2095) generally projects the coldest night of the year (TNn) to be warmer across the northern hemisphere compared to the present climate (BASE; 2010-2030), and cooler in the southern hemisphere with the exception of Antarctica relative to BASE (see Figure 2a, Figure 3 and Figure S1). Reduction of the coldest night temperature in GLENS EC is most noticeable across the tropics but is only in the order of 1°C and is not statistically significant. GLENS EC projects statistically significant increases in the temperature of the coldest night in Central Europe by up to 8°C; this increase is around half of that projected by RCP 8.5 EC. The strong winter warming in GLENS over Eurasia has been identified by others (Jiang et al., 2019; Tilmes et al., 2018) and has been linked to a strengthened northern hemisphere polar vortex (Banerjee et al. 2021). In contrast, GLENS coldest day of the year (TXn; Figure 2b, Supplemental Figures S2 and S3) projects a broad pattern of cooling

https://doi.org/10.5194/egusphere-2022-1
Preprint. Discussion started: 14 March 2022

across both hemispheres, with some statistically insignificant warming across the Sahara and the northern part of Canada; and significant (albeit marginal) cooling over Eurasia.

Similar to the coldest night, GLENS EC projects a pattern of warming for the warmest night (TNx) in the northern hemisphere and cooling in the southern hemisphere, with the exception of a cooler region in the northern part of Canada (Figure 2c, Supplemental Figures S4 and S5). However, GLENS EC projects significant warming over Antarctica, with cooling in other parts of the southern hemisphere. GLENS EC warmest day of the year (TXx; Figure 2d; Supplemental Figures S6 and S7) follows the same pattern of warming and cooling shown by TXn, with the greatest cooling occurring between 30°N-60°N of around -3°C; exceptions are northern Siberia and Canada. The warming in very high latitudes (>80°N or >80°S) arises from the implementation of the equator-to-pole temperature control in the feedback algorithm, whereby increased cooling in the high Arctic and Antarctica leads to warmer spots at slightly lower latitudes (Kravitz et al., 2017).

https://doi.org/10.5194/egusphere-2022-1
Preprint. Discussion started: 14 March 2022

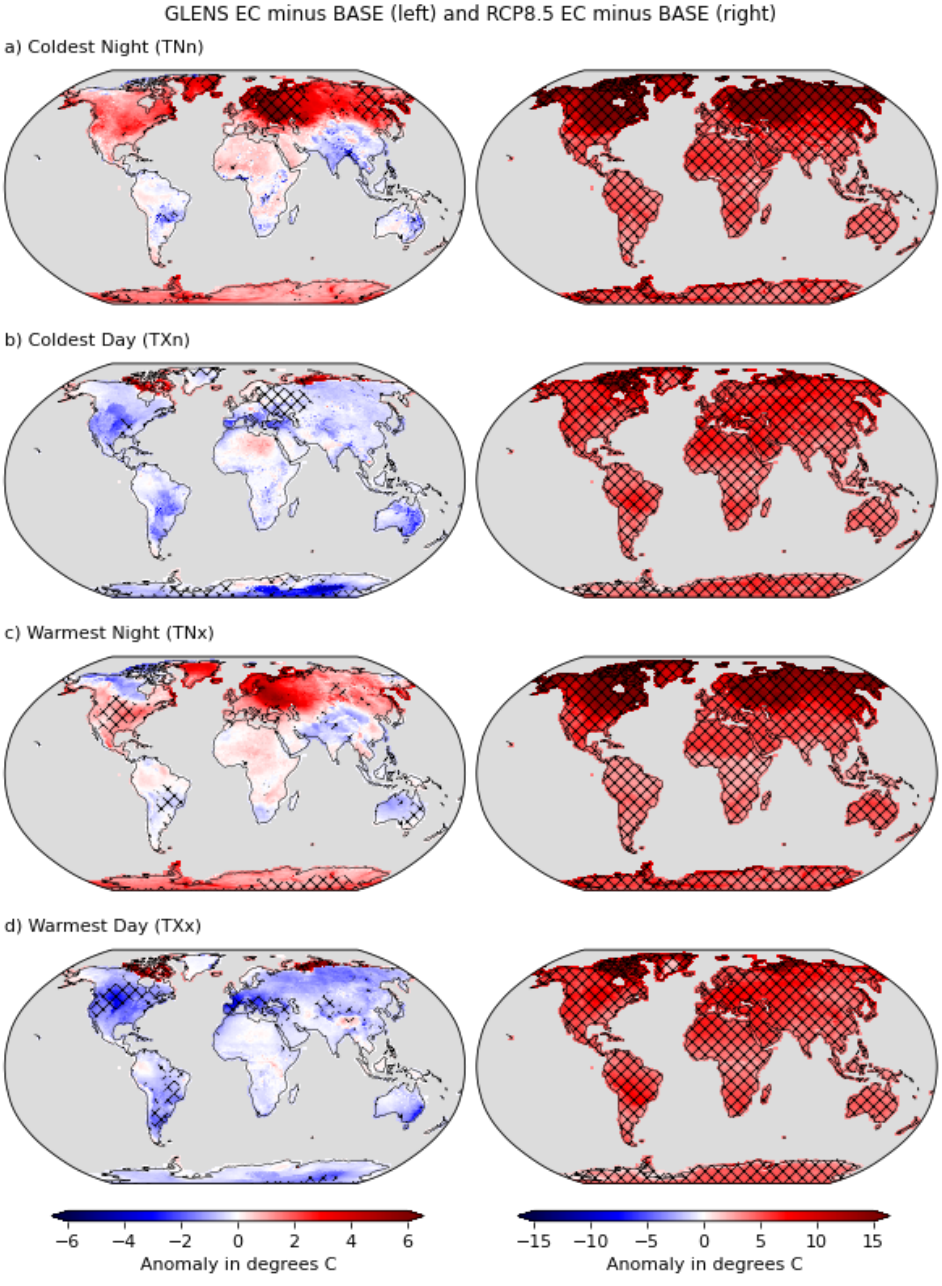

Figure 2: Projected anomalies between the GLENS EC scenario (2075-2095) and BASE (2010-2030) for annual coldest night and day (TNn, TXn), and warmest night and day (TNx, TXx) shown in the left column, and for anomalies between RCP8.5 EC (2075-2095) and BASE (2010-2030) shown in the right column. Note that the colorbar is different in the right column. Hatching indicates significance at the 5% test level using the Student's t-test.

https://doi.org/10.5194/egusphere-2022-1
Preprint. Discussion started: 14 March 2022

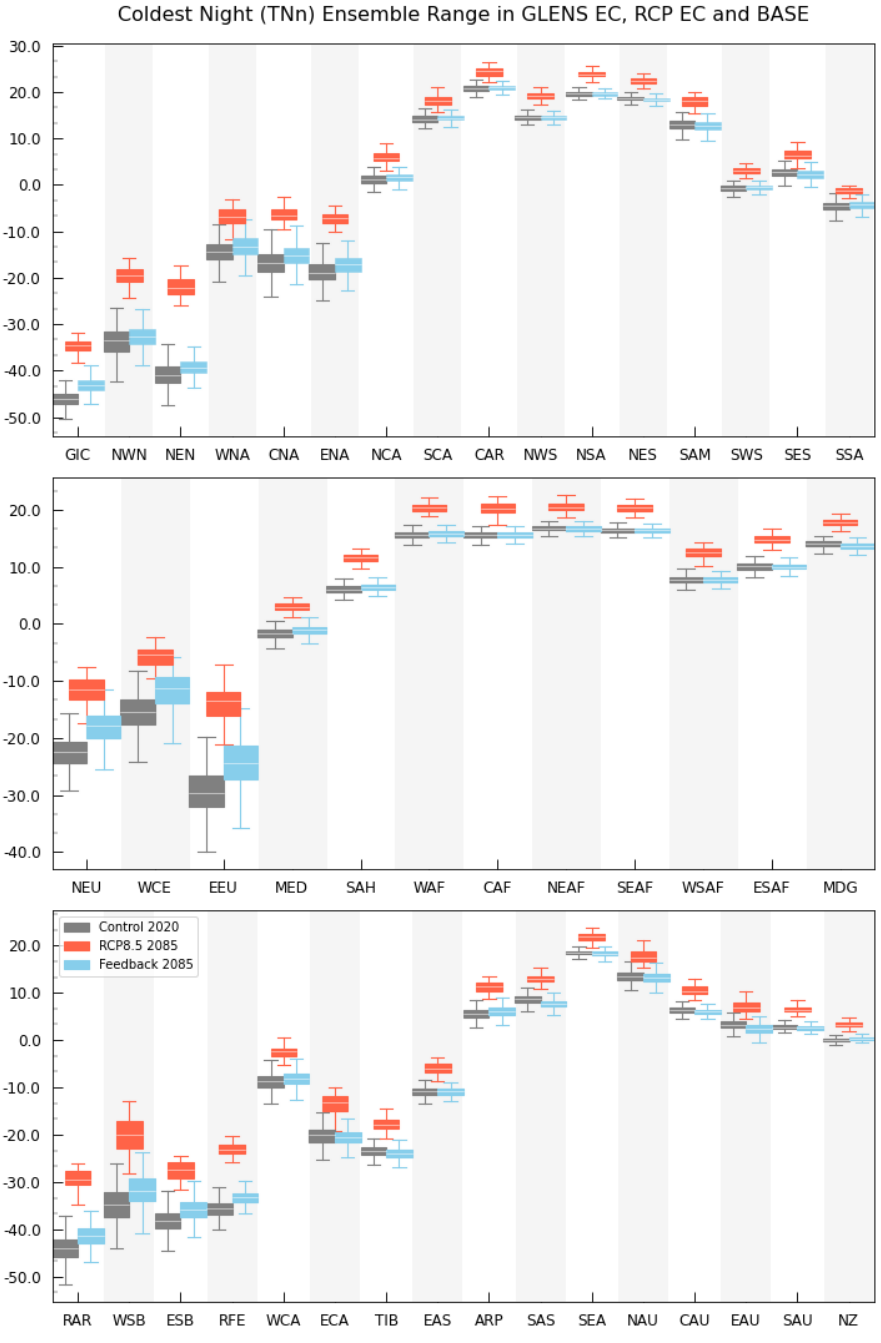

Figure 3: Climatological mean of coldest night (TNn) for: BASE (2010-2030) in grey, GLENS End of Century (EC; 2075-2095) in blue and RCP8.5 EC in red in each of the AR6 regions except Antarctica (Iturbide et al., 2019). Boxes show ensemble mean in white with the limits set at 25% and 75% of the ensemble spread; whiskers denote 5% and 95% ensemble spread.

https://doi.org/10.5194/egusphere-2022-1
Preprint. Discussion started: 14 March 2022

3.1.2 Fixed Thresholds

Changes in the number of nights with a minimum below 0°C (frost days; FD; Figure 4a, Supplemental Figures S8 and S9) may reflect considerable impacts for human and ecological health through changes in the frequency of daily minima below 0°C. In some regions, maintaining or increasing the frequency of the coldest days could be beneficial by suppressing the growth of pests or transmission of vector and zoonotic borne disease (e.g. Logan et al., 2010; Mills et al., 2010). However, colder temperatures in combination with other socio-economic factors can also increase the risk of winter mortality (Smith et al., 2014). Sillmann et al. (2013b) noted consistent decreases in the projected frequency of FD across all climate models and emissions scenarios. CESM1 RCP8.5 projections were amongst the largest decreases ranging from a global mean decrease of 30 days to over 100 days at high latitudes by the end of the century, as illustrated in the right column of Figure 4a.

The pattern of GLENS EC changes in FD (Figure 4a, left) differs in magnitude from RCP8.5 EC (Figure 4a, right) and includes some regions of increasing FD. Similar to projected changes in mean temperatures (Tilmes et al., 2018), GLENS EC projects cooler temperatures in the mountainous regions of Asia, with significant decreases in FD. Similarly, GLENS EC projects significant decreases in FD over northern Europe that also tally with projected changes in the frequency of cool nights (Supplemental Figures S10 and S11) and increases in TNn. Projections for the frequency of daily maxima below 0°C (ice days; ID) in GLENS EC are very similar to those of FD frequency, but are only statistically significant across Europe (decreases) and parts of Asia (increases). Refer to Figure 4b and Supplemental Figures S12 to S15, including contextual changes in the frequency of cold days.

Nighttime low temperatures exceeding 20°C (tropical nights, TR) are a potential indicator of health-related impacts in extratropical regions (Mitchell et al., 2016), and in many locations have been observed to increase more rapidly than daytime temperatures (Cox et al., 2020). Of note is the projected increase in frequency in TR over the Middle East and North Africa region (MENA) in GLENS (Figure 4c; Supplemental Figures S16 and S17) where other ETCCDI, including warm nights (Supplemental Figures S18 and S19), project little change or decrease in temperature. These increases are lower than those projected by RCP8.5 EC (Figure 4c, right). In a pattern noted above, the frequency of daytime temperatures exceeding 25°C (summer days, SU) generally decreases, particularly in the tropics (Figure 4d; Supplemental Figures S20 and S21). The main exception to this pattern is southern Africa where increases of SU up to 20 days are projected in GLENS. Localized patterns of warming and cooling have also been linked to changes in cloud cover, humidity and vegetative responses (Cox et al., 2020; Visioni et al., 2020), with the sulfate aerosols affecting medium altitude cloud formation more than

https://doi.org/10.5194/egusphere-2022-1
Preprint. Discussion started: 14 March 2022

climate related warming (Visioni et al., 2020). While GLENS EC projects increases in SU, the increases are still substantially lower than those projected by RCP8.5 EC (Figure 4d, right), and match the pattern of limited changes in daytime temperatures when compared to TXx and the frequency of hot days (Supplemental Figures S22 and S23).

https://doi.org/10.5194/egusphere-2022-1
Preprint. Discussion started: 14 March 2022

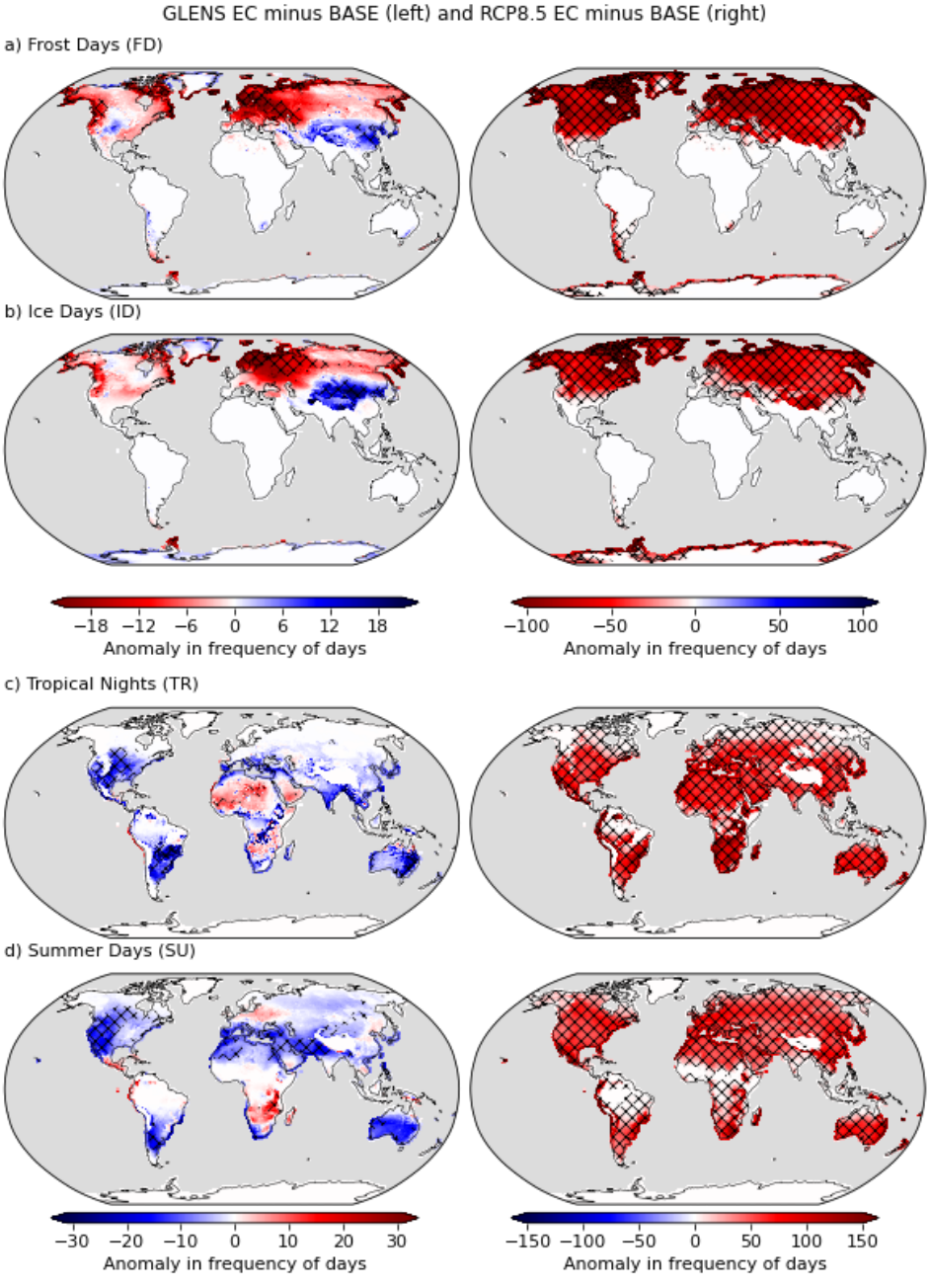

Figure 4: The same as Figure 2, but containing projected anomalies in the frequency of daily minima <0°C (frost days, FD), daily maxima <0°C (ice days, ID), daily minima >20°C (tropical nights, TR) and daily maxima >25°C (summer days, SU). Hatching indicates significance at the 5% test level using the Student's t-test.

https://doi.org/10.5194/egusphere-2022-1
Preprint. Discussion started: 14 March 2022

3.1.3 Temperature summary

While the changes in GLENS EC ETCCDI for temperature generally reflect the same spatial patterns as those reported for mean temperature (Tilmes et al., 2018; Cheng et al., 2021) there are some notable differences. Figure 5 compares the GLENS EC projected changes in mean temperature, in the center, against projected changes in the warmest night (TNx) for selected regions. In all cases, the time series are dominated by the increases in TNx for RCP8.5 EC. However, where large increases in the mean are projected over Europe in GLENS EC, the increases in TNx are minimal; in contrast, no change in the mean over Northeast North America is partnered by an increase in TNx. Climate change projections demonstrate that daily minimum temperatures (i.e. the nighttime low) often increase more rapidly than mean temperatures. While many increases are offset within GLENS EC, there are significant increases in the coldest night of the year (TNn) and decreased frequency of frost and ice days (FD, ID), in conjunction with the reported winter warming over Eurasia (Banerjee et al., 2021). GLENS EC also projects increases in the frequency of tropical nights (TR) over much of Africa and parts of Central America, although lower than the increases projected in RCP8.5 EC. The projected increase in annual maximum temperature (TXx) over northern India in GLENS EC is an interesting contrast to the projected cooling in this region, but is consistent with other research (Muthalya et al. 2018b; Irvine et al., 2019). As discussed below, the warming over the Tibetan Plateau and northern India is linked to changes in monsoonal rain (Visioni et al., 2019).

We note that many of the projected increases in temperature extremes in GLENS EC are not statistically significant with respect to the current climate (BASE). This is a positive result, demonstrating that the mean climate state has been maintained at the nominal BASE climate in this set of simulations. However, these simulations represent only one snapshot of the potential response to SAI, other simulations that commence at a different time period, or use different feedback controls may show other results. Furthermore, changes in the hydrological cycle and vegetative responses may be very different from changes in temperature; as discussed in Sect. 3.2 and 3.3.

https://doi.org/10.5194/egusphere-2022-1
Preprint. Discussion started: 14 March 2022

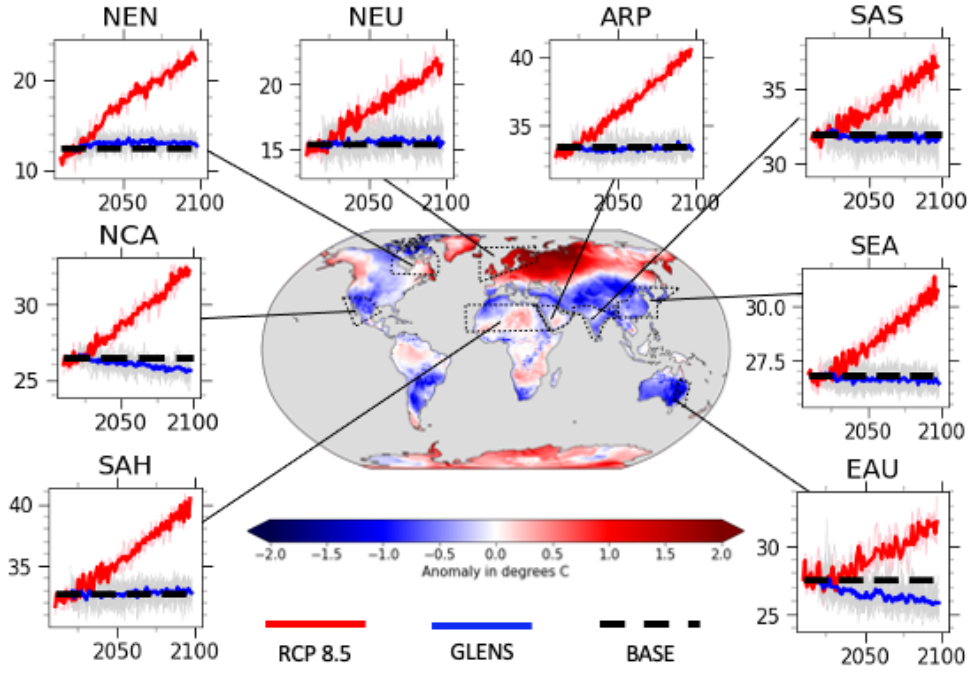

Figure 5: Ensemble mean of projected changes in mean global temperature for GLENS EC (2075-2095) minus BASE (2010-2030) with inset regional time series of the warmest night (TNx) for Northeast North America (NEN), North Central America (NCA), Sahara (SAH), North Europe (NEU), Arabian Peninsula (ARP), South Asia (SAS), East Asia (EAS) and East Australia (EAU).

3.2 Precipitation

Considerable variation in precipitation patterns tends to overwhelm any emergent climate signal, such that many of the changes discussed below are not statistically significant. Even though we are examining end of the century changes (2075-2095), the differences are often not distinguishable from variability until the second half of the climate period (i.e. 2085-2095).

3.2.1 Fixed Indices

GLENS EC (2075-2095) global mean precipitation over land is projected to change very little with respect to BASE (2010-2030; Cheng et al., 2019; Simpson et al., 2019). However, there are spatial variations in this pattern that relate to orographic and oceanic processes, in addition to seasonal variations. For example, Simpson et al. (2019) reported a decrease in annual total precipitation (PRCPTOT) in regions where the mean daily precipitation ≥ 5mm/day, with reductions over land affecting India, Indonesia and northeastern South America and increases over central Australia. As with temperatures, a strong seasonal signal is apparent that affects the intensity of

https://doi.org/10.5194/egusphere-2022-1
Preprint. Discussion started: 14 March 2022

312 GLENS projected increases and decreases. The patterns of change in GLENS annual mean precipitation are
313 accentuated during the northern hemisphere summer (JJA) and linked to a reduction in the east-west gradient of
314 Pacific SSTs (Simpson et al., 2019). In contrast, those same regions are projected to experience little to no change
315 during the northern hemisphere winter (DJF), while Indonesia and the northern territories of Australia are
316 projected to experience increased precipitation. Again, this is linked to changes in the east-west gradient of Pacific
317 SSTs (Simpson et al., 2019; Trisos et al., 2018).

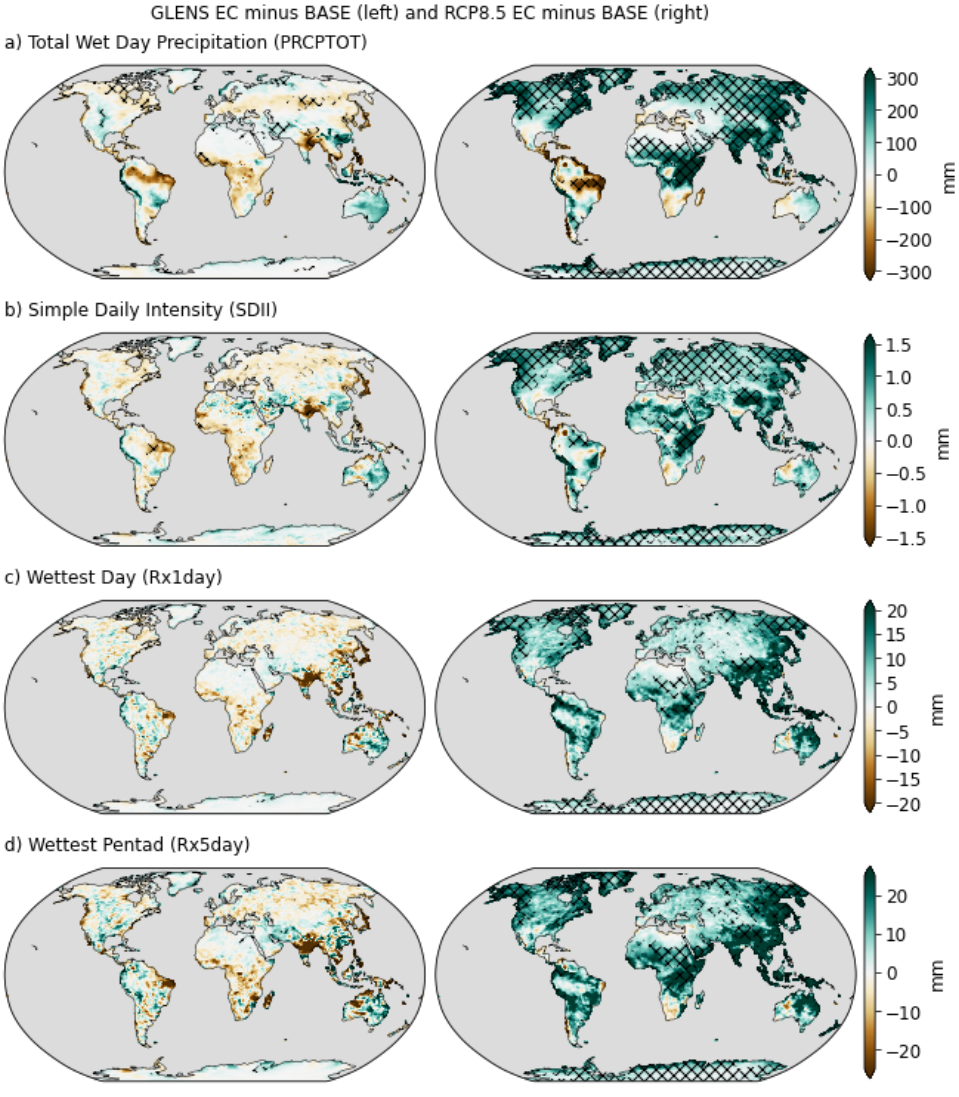

318

https://doi.org/10.5194/egusphere-2022-1
Preprint. Discussion started: 14 March 2022

Figure 6: Similar to Figure 2, but for projected changes in a) annual precipitation (PRCPTOT), b) the mean wet day volume (SDII), c) annual maximum precipitation (Rx1day), and d) annual wettest pentad (Rx5day). Hatching indicates significance at the 5% test level using the Student's t-test.

GLENS EC projected changes in PRCPTOT (Figure 6a; Supplemental Figures S24 and S25) relative to BASE show little spatial change except in the tropics, and in general few of those changes are statistically significant. One of the few regions to project significant change in PRCPTOT is the coastal part of West Africa, where the decreases are on the order of 300mm per year. Other regions project increases and decreases that replicate the general pattern of "wet gets drier/dry gets wetter" reported by Simpson et al. (2019), and with considerable year-to-year variability. Haywood et al. (2013) reported a contraction in the intertropical convergence zone (ITCZ) in geoengineering simulations that corresponds with the projected changes in annual moisture patterns. The simple daily intensity, or mean wet day total (SDII; Figure 6b, Supplemental Figures S26 and S27), starts to illustrate that the projected increases and decreases in PRCPTOT in GLENS arise from a change in the number of days with precipitation, not only the intensity on those days. For instance, parts of Western Australia, the MENA and southern China project increases in SDII in GLENS where little or no change is projected in PRCPTOT by GLENS EC.

The greatest projected decreases in annual total precipitation within the ITCZ are, with the exception of the Indian Monsoon region, projected to have little or no change in the annual wettest day (Rx1day; Figure 6c, Supplemental Figures 28 and 29) and wettest pentad (Rx5day; Figure 6d, Supplemental Figures 30 and 31). In contrast, RCP8.5 EC projects significant increases in PRCPTOT across much of the globe that are largely driven by increases in the most intense few events per year (Figure 6, right). Under the RCP8.5 EC scenario there is projected to be greater volatility in the distribution of days with precipitation, such that even regions that are projected to dry will also experience more intense extreme events (e.g. north South America). This contrasts with GLENS EC where changes in PRCPTOT and the most extreme events appear to move in the same direction (i.e. decreases in Rx1day, and lower PRCPTOT), leading to a more uniform distribution of precipitation.

The most striking change in GLENS is the projected drying over the northern part of India and Bangladesh, with changes in all extreme precipitation ETCCDI. GLENS projects decreases in annual maxima over northern India (Figure 6c) that are approximately co-located with projected cooling compared to BASE (e.g. Figure 5), thus following the Clausius-Clapeyron curve. The related decreases in soil moisture and latent heat flux over northern India in GLENS are discussed further in Section 4.3. This has been linked to the seasonality of temperature changes over the Tibetan Plateau in response to annual rather than seasonal injection strategies, resulting in changes in the monsoon precipitation (Visioni et al., 2019).

https://doi.org/10.5194/egusphere-2022-1
Preprint. Discussion started: 14 March 2022

3.2.2 Spells

Regions with projected decreases in PRCPTOT under RCP8.5 EC tend to project increases in the duration of the longest dry spells (CDD) and decreases in the duration of wet spells, (CWD; Sillmann et al., 2013b; Giorgi et al., 2014) shown in Figure 7 (right column). However, GLENS EC projections of CDD (Figure 7a; Supplemental Figures S32 and S33) and CWD (Figure 7b; Supplemental Figures S34 and S35) are more complicated, with lower apparent correlation between changes in the longest dry and wet spells and changes in PRCPTOT. Given that other metrics (SDII, Rx1Day, R10mm) indicate changes in frequency and intensity affect PRCPTOT, this suggests that dry day persistence decreases in GLENS EC in contrast with the increases found for non-SAI projections (Giorgi et al., 2019). Furthermore, increases or decreases in the longest dry spell do not necessarily correspond to changes in the longest wet spell (CWD). Projected decreases in the longest dry spell over the Sahara and Middle East (SAR, EAP) in GLENS EC are considerable but not statistically significant, and as noted by Pinto et al. (2020) these are accompanied by increases in the south east (SEAF, ESAF) and highlight the dichotomy of regions that benefit from, or are further disadvantaged by, SAI.

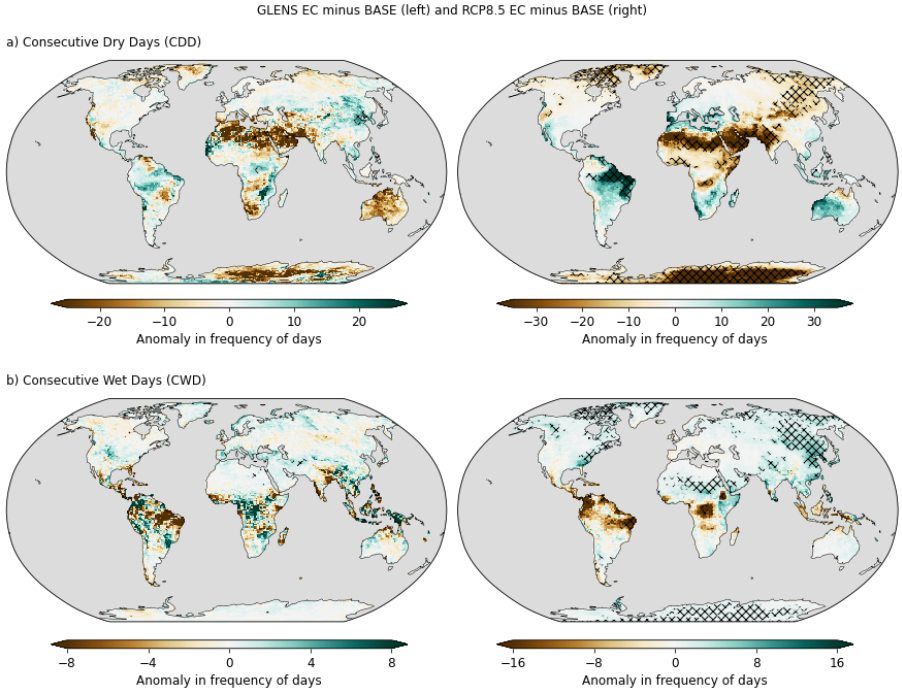

Figure 7: Similar to Figure 2, but for projected changes in a) the longest spell of dry days (CDD) and b) longest spell of wet days (CWD). Hatching indicates significance at the 5% test level using the Student's t-test.

https://doi.org/10.5194/egusphere-2022-1
Preprint. Discussion started: 14 March 2022

3.2.3 Fixed Thresholds

Projected changes in GLENS and RCP8.5 in the frequency of heavy (R10mm) and very heavy (R20mm) precipitation days are shown in Figure 8 (and Supplemental Figures S36-S39). Within the ITCZ, where SDII is near to 10mm/day, the pattern of projected changes in GLENS EC (Figure 8, left) is very similar to that of other metrics and indicates that the changes are proportional across the precipitation intensity distribution. Outside the ITCZ, GLENS EC projects a less disproportional shift than projected by RCP8.5. That is, wet regions may become wetter, but not as a result of precipitation falling in fewer more intense events. Thus, regions such as northeastern South America and northeastern India that have considerable projected decreases in PRCPTOT under GLENS also have projected decreases in the number of R10mm and R20mm days, but not in the duration of the longest wet and dry spells. Similarly, the GLENS EC projected increase in PRCPTOT over Indonesia is related to projected increases in heavy precipitation days and not to the intensity of the most extreme events (Rx1day, Rx5day). The projected increases and decreases in R10mm and R20mm also correspond to the projected increases and decreases in the annual maximum temperatures (TXx; Figure 2), as anticipated under the Clausius-Clapeyron relationship.

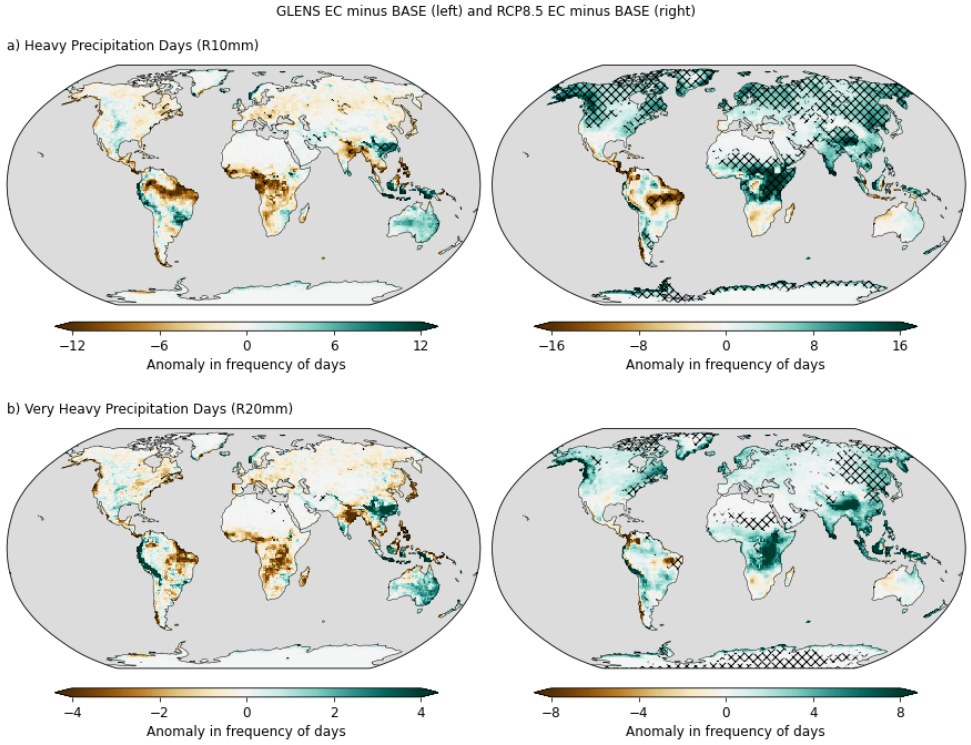

Figure 8: Similar to Figure 2, but for projected changes in a) the frequency of days with heavy precipitation (R10mm)

https://doi.org/10.5194/egusphere-2022-1
Preprint. Discussion started: 14 March 2022

and b) days with very heavy precipitation (R20mm). Hatching indicates significance at the 5% test level using the Student's t-test.

3.2.4 Precipitation summary

As with temperature, patterns for the precipitation ETCCDI are very similar to those seen in GLENS EC mean precipitation (Simpson et al., 2019), but the changes are not uniform across all indices or all locations. Figure 9 illustrates the change in mean precipitation between GLENS EC and BASE (Simpson et al., 2019) together with projected changes in the frequency of heavy rain days (R10mm) for several regions. While GLENS EC generally projects increases in precipitation where RCP8.5 EC projects decreases, and vice versa, there are some exceptions to this pattern. In particular, some parts of South America and Africa are projected to experience enhanced drying compared to BASE under both GLENS EC and RCP8.5 EC (Cheng et al., 2019; Simpson et al., 2019; Pinto et al., 2020) and is discussed further in the context of vegetative responses in Section 4. However, we find that many of the projected changes in GLENS EC are not statistically significant when compared to the current climate.

GLENS EC changes in PRCPTOT are related in part to changes in the intensity on the wettest days, but also to the frequency of days with precipitation. For instance, the greatest projected decreases in PRCPTOT within the ITCZ are accompanied by projected decreases in the number of days with more than 10mm precipitation (R10; Figure 8a). That is, there is a shift towards more days with less intense rain and fewer very intense rain days consistent with other experiments (Ji et al., 2018). Changes in the heavier events also follow the anticipated changes from Clausius Clapeyron, where changes in Rx1day largely correspond with changes in temperature (Figure 5).

https://doi.org/10.5194/egusphere-2022-1
Preprint. Discussion started: 14 March 2022

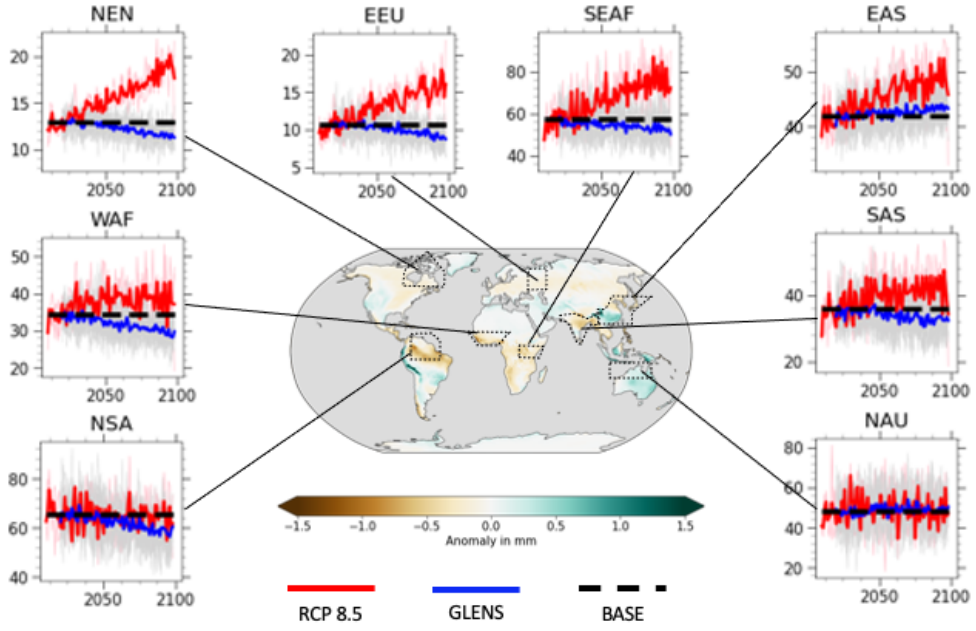

Figure 9: Ensemble mean of projected changes in mean daily precipitation for GLENS EC (2075-2095) minus BASE (2010-2030) with inset regional time series of frequency of days >10mm (R10mm) for Northeast North America (NEN), North South America (NSA), South Eastern Africa (SES), Western Africa (WAF), Eastern Europe (EEU), South Asia (SAS), East Asia (EAS) and North Australia (NAU).

4 Vegetation response

We focus on three regions where the GLENS responses of soil moisture, vegetation and evapotranspiration are very different, despite similarities in the projected temperature and precipitation. These regions further emphasize that despite the ability to maintain global mean temperature and precipitation at a target level, the effects of climate change cannot be completely offset and will have regional and temporal differences that could be considerable (Jones et al., 2018; Simpson et al., 2019; Tilmes et al., 2013). The three regions of interest are North and Northeast South America, Western and Central Africa, and India (South Asia in AR6 regions), and are marked on Figures 10 and 11. All of these regions have been highlighted as sensitive to the effects of changes in the hydrological cycle under SAI (Bhowmick et al., 2021; Da Allada et al., 2020; Jones et al., 2018; Pinto et al., 2020; Simpson et al., 2019). GLENS projects decreases in latent heat flux (LHF; Figure 10a), together with increases in leaf area index (LAI; Figure 10c) and gross primary production (GPP; Figure 10d) in all three regions, but with different partitioning of the water fluxes (Figure 11) related to soil moisture at the surface (SM10; Figure 10b) and temperature.

https://doi.org/10.5194/egusphere-2022-1
Preprint. Discussion started: 14 March 2022

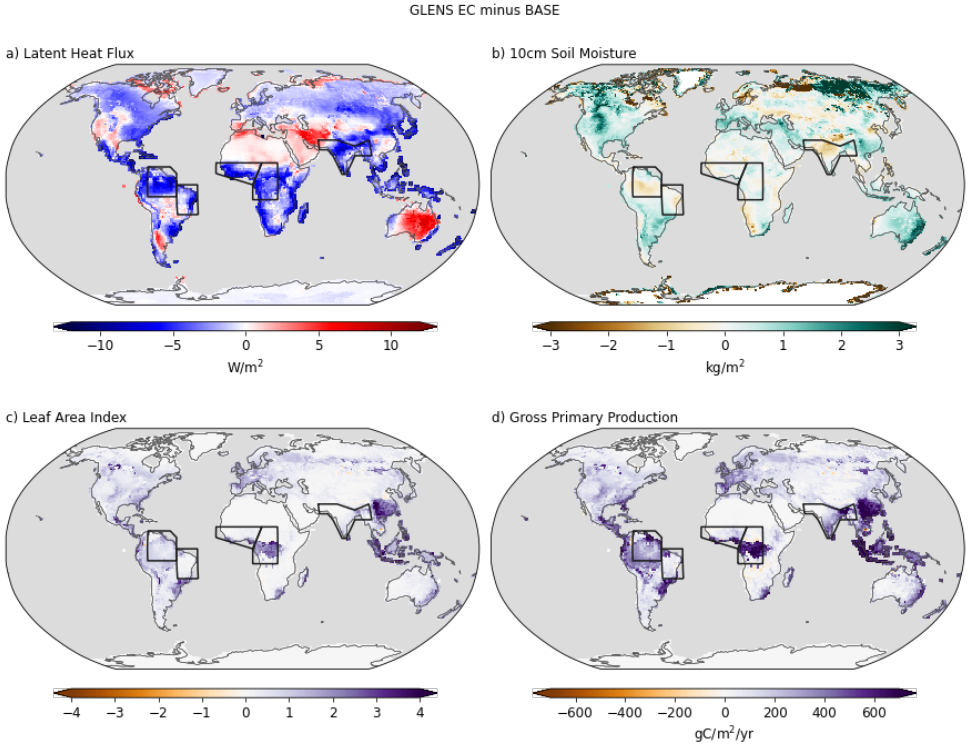

Figure 10: Projected changes between GLENS EC (2075-2095) and BASE (2010-2030) in a) latent heat flux; b) soil moisture in the top 10cm; c) total leaf area index; and d) gross primary production. Black polygons highlight the following regions: Northeast South America (NSA), North South America, Western Africa (WAF), Central Africa (CAF), and South Asia (SAS).

https://doi.org/10.5194/egusphere-2022-1
Preprint. Discussion started: 14 March 2022

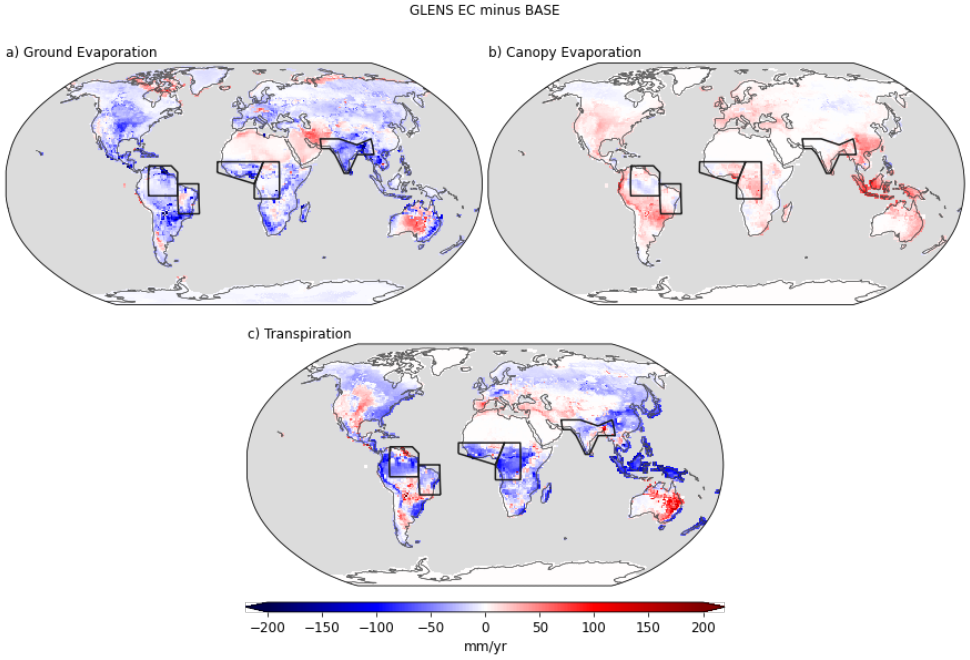

Figure 11: Projected changes between GLENS EC (2075-2095) and BASE (2010-2030) in a) ground evaporation, b) canopy evaporation, and c) transpiration. Highlighted regions as for Figure 10.

4.1 North and Northeast South America

The Amazon basin is projected to dry considerably under unmitigated climate change, with changes in evapotranspiration playing a large part in the hydrological cycle changes (Halladay and Good, 2017). Other research has also identified that SAI may offset some of the projected drying but not the full effects (Cheng et al., 2020; Simpson et al., 2019), with plant feedbacks identified as the main contributing factor (Jones et al., 2018; Xia et al., 2016).

The GLENS projected decreases in mean precipitation occur across the full distribution of precipitation, with resultant decreases in soil moisture (Figure 10b). These decreases are accompanied by different rates of change in the daytime (TX) and nighttime (TN) temperatures with increases in TN but decreases in TX (see Figures 2 and 5). Changes in all three metrics correlate with the posited relationship between cloud cover, vegetation, precipitation and differential warming (Cox et al., 2020) and reflect the potential for increases in cloud cover (Krishnamohan and Bala, 2022; Visioni et al., 2021). The projected change in water flux partitioning appears to be linked to the change in persistence of wet and dry periods. That is, increases in vegetation shown by LAI along with increases in atmospheric CO_2 lead to more efficiency in water recycling with less ground evaporation (Figure

https://doi.org/10.5194/egusphere-2022-1
Preprint. Discussion started: 14 March 2022

11a) and transpiration (Figure 11c), but more canopy evaporation in parts of the region (Figure 11b), coupled with lower atmospheric moisture content and shorter wet spells (CWD).

4.2 Western and Central Africa

RCP8.5 EC precipitation patterns over the Sahel, Central and Western Africa are likely to be more extremely distributed, with increased intensity of the wettest days, longer dry spells and shorter wet spells. Similar to the Amazon basin, GLENS EC appears to offset some of the extremes in temperature and precipitation projected by RCP8.5 EC over the Sahel, but would likely lead to decreases in precipitation over Western Africa and Southern Africa (Da-Allada et al., 2021; Pinto et al., 2020). The greatest increase in LAI and associated GPP (Figure 10c-d) in GLENS are also accompanied by warmer days and cooler nights (Figures 4 and 5) but decreases in mean and extreme precipitation (Figures 6 and 9). This largely follows the anticipated asymmetric diel warming relationships (Cox et al., 2020) and corroborates potential reductions in cloud cover (Krishnamohan and Bala, 2022; Visioni et al., 2021) together with increased persistence of dry spells (Pinto et al., 2020). As with other locations in the tropics, the decreases in LHF are also driven primarily by decreases in transpiration (Figure 11c; Dagon and Schrag, 2019).

4.3 India (South Asia)

The regional reductions in extreme precipitation metrics, i.e. drying, over India are confirmed by examining changes in latent heat flux and soil moisture (Figure 10a-b). Away from the tropics, LHF is dominated by ground evaporation and soil moisture - both of which decrease in the GLENS EC projections. The reduction in LHF is likely also linked to reductions in cloud cover (Krishnamohan and Bala, 2022; Visioni et al., 2021). However, there is little change in LAI or canopy evaporation, coupled with a slight increase in the asymmetry of increasing TX versus decreasing TN in GLENS EC (Refer to Section 3.1, and Figures 2 and 5). The changes in all precipitation ETCCDI over India are most closely related to the changes in mean JJA precipitation, and hence the summer monsoon, with variability in the ITCZ and differential temperature gradients over the Tibetan Plateau playing a large role (Bhowmic et al., 2021; Visioni et al., 2020).

4.4 Vegetation Summary

The contrast in vegetative responses in these three regions emphasizes that several different mechanisms can be responsible for regional drying under SAI. Jones et al. (2018) hypothesized three principal mechanisms that relate

https://doi.org/10.5194/egusphere-2022-1
Preprint. Discussion started: 14 March 2022

to changes in the hydrological cycle: an increased tendency for the ITCZ to favor the warmer hemisphere (India); changes in SST over the Atlantic and Western Pacific that mimic an El Niño like response (Western and Central Africa); or plant physiological responses (North and Northeast South America). Similar to Jones et al. (2018), our results show that the main driver of Amazon drying, and likely other highly vegetated regions in the tropics, is the response of vegetation to increased CO_2 through more efficient water use and enhanced transpiration, and cloud development. Over India the contrast between day and night temperatures has the opposite effect on cloud generation, with accompanying decreases in precipitation but less obvious changes in the vegetation growth. On the other hand, the increase in GPP demonstrates an increase in water use efficiency that balances the heat stress experienced by plants. This suggests that drying over India is more closely related to the temperature gradients influenced by the equatorward shift of water transporting systems than specific changes in vegetative behavior. Drying over Central and Western Africa reflects a combination of diel asymmetry in warming with reduced cloud coverage, and increased plant feedbacks exacerbating the drier conditions.

5 Conclusions

SAI has been suggested as a possible mechanism to moderate some of the effects of climate change while more long term and robust strategies to phase-out anthropogenic carbon emissions take effect (Keith and Irvine, 2016; MacMartin et al., 2018; Tilmes et al., 2020; Honegger et al., 2021). It is also widely acknowledged that such a measure will bring benefits and disadvantages, thus necessitating a proper assessment of the different tradeoffs and risks (Kravitz et al., 2021; Florin, 2021). To contribute to that discussion, we presented an assessment of the anticipated changes to temperature and precipitation ETCCDI indices, and associated vegetation responses, under a geoengineering scenario intended to moderate the extreme climatic changes expected under RCP8.5. This ensemble explicitly simulates the responses from aerosols and offers the opportunity to determine whether the responses are distinguishable from internal variability.

We find that GLENS is generally successful at maintaining mean temperature and mean precipitation near 2020 levels. Where GLENS EC either does not offset, or is too aggressive in compensating, projected changes in ETCCDI under RCP8.5 EC, the changes are similar to those reported for mean temperature and mean precipitation (Tilmes et al., 2018; Simpson et al., 2019; Cheng et al., 2021). Furthermore, many of the projected changes in ETCCDI in GLENS EC are not significantly different from the simulated current climate (BASE), indicating that SAI could offset the worst effects projected by RCP8.5 EC. However, we also note that SAI is preferentially more effective for daytime temperatures than nighttime due to the reduction in incoming solar irradiation, resulting in

https://doi.org/10.5194/egusphere-2022-1
Preprint. Discussion started: 14 March 2022

warmer minimum temperatures and cooler maximum temperatures (Curry et al., 2014; Malik et al., 2020). In addition to the winter warming over Europe, North America and Asia (Banerjee et al., 2021), our results indicate asymmetric increases in warm nights (TNx, TR) compared to cooler days in the summer (TXx, SU). GLENS EC projects increases in warm nights over northern India which contrast with the projected cooling in mean temperatures (Tilmes et al., 2018), but is consistent with other research (Muthalya et al. 2018b; Irvine et al., 2019) and is likely driven by seasonal variations in the ocean-land temperature contrasts (Visioni et al., 2020; Krishnamohan and Bala, 2022). Furthermore, the projected amplitude of changes is greater at higher latitudes even though the changes scale with global mean temperatures (Kharin et al., 2018).

The asymmetry of changes in warm and cool events has been linked to a contraction or shift in the Intertropical Convergence Zone in other geoengineering simulations (Haywood et al., 2013; Krishnamohan and Bala, 2022). Changes in the frequency and strength of El Niño and La Niña events as a result of SAI are difficult to confirm (Gabriel and Robock, 2015). However, GLENS EC projected equatorward shifts in westerlies and storm tracks (Karami et al., 2020), together with increasing precipitation over Australia and weakening of the African and Indian Monsoons (Da Allada et al., 2020; Bhowmick et al., 2021) support a weakened ENSO signal compared to present day (Malik et al., 2020). In keeping with these results, we find that projected changes in the annual total precipitation in GLENS arise from a change in the number of days with precipitation, not only the intensity on those days. Thus, GLENS EC projects precipitation on more days with fewer very intense events.

Vegetation responses are very sensitive to changes in precipitation and temperature. In particular contrasting rates of change in day and night temperatures play a large role in the development of clouds and vegetation responses (Cox et al., 2020). We find that GLENS projected increases in leaf area index within the tropics are associated with increases in nighttime temperatures and decreased precipitation extremes. These also correspond to reductions in latent heat flux (LHF) that are dominated by the decreases in transpiration as a result of carbon cycle feedbacks (Dagon and Schrag, 2019). However, in regions where the changes in LHF are dominated by soil moisture and ground evaporation, the projected drying is accompanied by little change in vegetation and is likely a response to changes in ocean-land temperature contrasts (Visioni et al., 2020; Krishnamohan and Bala, 2022). A similarly complicated picture of drying over central and western Africa relates to the GLENS projected reductions in cloud cover, asymmetric warming and increased plant feedbacks compared to present day conditions. While we did not examine it explicitly, the integrated responses of diurnal temperatures, precipitation and vegetative responses are likely the explanation for spatially inconsistent changes in soil moisture and evapotranspiration (Cheng et al., 2018) and will be the focus of future study.

https://doi.org/10.5194/egusphere-2022-1
Preprint. Discussion started: 14 March 2022

Supplement

See separate file for supplemental figures.

Code and Data Availability

The ETCCDI were calculated in Python using the xclim package in addition to other standard imported packages. The original definitions of ETCCDI are available from http://etccdi.pacificclimate.org/list_27_indices.shtml. The code is available on request from maritye@ucar.edu. The Geoengineering Large Ensemble Data are available via the Earth System Grid at http://doi.org/10.5065/D6JH3JXX and described at https://www.cesm.ucar.edu/projects/community-projects/GLENS/.

Author Contributions

MT, JR, and CT conceived the analysis. MT performed the analysis with assistance from KD, MM, JR and DV. MT wrote the paper with contributions from all authors.

Competing Interests

MT, KD, MM, JR, DV, CT and ST declare no competing interests. BK is a member of the editorial board for Earth System Dynamics. The peer-review process was guided by an independent editor and BK has no other competing interests to declare.

Acknowledgements

We thank John Fasullo, Christine Shields, and Lili Xia for their useful conversations that informed this work. This material is based upon work supported by the National Center for Atmospheric Research, which is a major facility sponsored by the National Science Foundation (NSF) under Cooperative Agreement No. 1852977. The CESM project is supported by the NSF. Computing and data storage resources, including the Cheyenne supercomputer (doi:10.5065/D6RX99HX), were provided by the Computational and Information Systems Laboratory (CISL) at NCAR. We thank all the scientists, software engineers, and administrators who contributed to the development of CESM1(WACCM).

https://doi.org/10.5194/egusphere-2022-1
Preprint. Discussion started: 14 March 2022

MT, KD and MM were supported by SilverLining through its Safe Climate Research Initiative. Support for Daniele Visioni was provided by the Atkinson Center for a Sustainable Future at Cornell University.

Support for BK was provided in part by the National Science Foundation through agreement CBET-1931641, the Indiana University Environmental Resilience Institute, and the *Prepared for Environmental Change* Grand Challenge initiative. The Pacific Northwest National Laboratory is operated for the US Department of Energy by Battelle Memorial Institute under contract DE-AC05-76RL01830.

References

Alexander, L. V., Bador, M., Roca, R., Contractor, S., Donat, M. G., & Nguyen, P. L. (2020). Intercomparison of annual precipitation indices and extremes over global land areas from in situ, space-based and reanalysis products. Environmental Research Letters, 15(5), 055002. https://doi.org/10.1088/1748-9326/ab79e2

Alexander, L. V., Zhang, X., Peterson, T. C., Caesar, J., Gleason, B., Klein Tank, A. M. G., Haylock, M., Collins, D., Trewin, B., Rahimzadeh, F., Tagipour, A., Rupa Kumar, K., Revadekar, J., Griffiths, G., Vincent, L., Stephenson, D. B., Burn, J., Aguilar, E., Brunet, M., … Vazquez-Aguirre, J. L. (2006). Global observed changes in daily climate extremes of temperature and precipitation. Journal of Geophysical Research, 111(D5), D05109. https://doi.org/10.1029/2005JD006290

Allan, R. P., Barlow, M., Byrne, M. P., Cherchi, A., Douville, H., Fowler, H. J., Gan, T. Y., Pendergrass, A. G., Rosenfeld, D., Swann, A. L. S., Wilcox, L. J., & Zolina, O. (2020). Advances in understanding large-scale responses of the water cycle to climate change. Annals of the New York Academy of Sciences, 1472(1), 49–75. https://doi.org/10.1111/nyas.14337

Allen, M. R., & Ingram, W. J. (2002). Constraints on future changes in climate and the hydrologic cycle. Nature, 419(6903), 228–232. https://doi.org/10.1038/nature01092

Asadieh, B., & Krakauer, N. Y. (2015). Global trends in extreme precipitation: Climate models versus observations. Hydrology and Earth System Sciences, 19(2), 877–891. https://doi.org/10.5194/hess-19-877-2015

Aswathy, V. N., Boucher, O., Quaas, M., Niemeier, U., Muri, H., Mülmenstädt, J., & Quaas, J. (2015). Climate extremes in multi-model simulations of stratospheric aerosol and marine cloud brightening climate

https://doi.org/10.5194/egusphere-2022-1
Preprint. Discussion started: 14 March 2022

engineering. Atmospheric Chemistry and Physics, 15(16), 9593–9610. https://doi.org/10.5194/acp-15-9593-2015

Banerjee, A., Butler, A. H., Polvani, L. M., Robock, A., Simpson, I. R., & Sun, L. (2021). Robust winter warming over Eurasia under stratospheric sulfate geoengineering – the role of stratospheric dynamics. Atmospheric Chemistry and Physics, 21(9), 6985–6997. https://doi.org/10.5194/acp-21-6985-2021

Bhowmick, M., Mishra, S. K., Kravitz, B., Sahany, S., & Salunke, P. (2021). Response of the Indian summer monsoon to global warming, solar geoengineering and its termination. Scientific Reports, 11(1), 9791. https://doi.org/10.1038/s41598-021-89249-6

Budyko, M. I. (1977). Climatic Changes. American Geophysical Union. https://doi.org/10.1029/SP010

Carlson, C. J., & Trisos, C. H. (2018). Climate engineering needs a clean bill of health. Nature Climate Change, 8(10), 843–845. https://doi.org/10.1038/s41558-018-0294-7

Cheng, W., MacMartin, D. G., Dagon, K., Kravitz, B., Tilmes, S., Richter, J. H., Mills, M. J., & Simpson, I. R. (2019). Soil Moisture and Other Hydrological Changes in a Stratospheric Aerosol Geoengineering Large Ensemble. Journal of Geophysical Research: Atmospheres, 124(23), 12773–12793. https://doi.org/10.1029/2018JD030237

Cox, D. T. C., Maclean, I. M. D., Gardner, A. S., & Gaston, K. J. (2020). Global variation in diurnal asymmetry in temperature, cloud cover, specific humidity and precipitation and its association with leaf area index. Global Change Biology, 26(12), 7099–7111. https://doi.org/10.1111/gcb.15336

Curry, C. L., Sillmann, J., Bronaugh, D., Alterskjaer, K., Cole, J. N. S., Ji, D., Kravitz, B., Kristjánsson, J. E., Moore, J. C., Muri, H., Niemeier, U., Robock, A., Tilmes, S., & Yang, S. (2014). A multimodel examination of climate extremes in an idealized geoengineering experiment. Journal of Geophysical Research: Atmospheres, 119(7), 3900–3923. https://doi.org/10.1002/2013JD020648

Da-Allada, C. Y., Baloïtcha, E., Alamou, E. A., Awo, F. M., Bonou, F., Pomalegni, Y., Biao, E. I., Obada, E., Zandagba, J. E., Tilmes, S., & Irvine, P. J. (2020). Changes in West African Summer Monsoon Precipitation Under Stratospheric Aerosol Geoengineering. Earth's Future. https://doi.org/10.1029/2020EF001595

Dagon, K., & Schrag, D. P. (2016). Exploring the Effects of Solar Radiation Management on Water Cycling in a Coupled Land-Atmosphere Model. Journal of Climate, 29, 2635-2650. http://dx.doi.org/10.1175/JCLI-D-15-0472.1

https://doi.org/10.5194/egusphere-2022-1
Preprint. Discussion started: 14 March 2022

604 Dagon, K., & Schrag, D. P. (2017). Regional Climate Variability Under Model Simulations of Solar
605 Geoengineering. Journal of Geophysical Research: Atmospheres, 122(22), 12,106-12,121.
606 https://doi.org/10.1002/2017JD027110

607 Dagon, K., & Schrag, D. P. (2019). Quantifying the effects of solar geoengineering on vegetation. Climatic
608 Change, 153(1–2), 235–251. https://doi.org/10.1007/s10584-019-02387-9

609 Diffenbaugh, N. S., & Giorgi, F. (2012). Climate change hotspots in the CMIP5 global climate model ensemble.
610 Climatic Change, 114(3–4), 813–822. https://doi.org/10.1007/s10584-012-0570-x

611 Donat, M. G., Sillmann, J., & Fischer, E. M. (2020). Changes in climate extremes in observations and climate
612 model simulations. From the past to the future. In J. Sillmann, S. Sippel, & S. Russo (Eds.), Climate
613 Extremes and Their Implications for Impact and Risk Assessment (pp. 31–57). Elsevier.
614 https://doi.org/10.1016/B978-0-12-814895-2.00003-3

615 Duan, L., Cao, L., Bala, G., & Caldeira, K. (2019). Climate Response to Pulse Versus Sustained Stratospheric
616 Aerosol Forcing. Geophysical Research Letters, 46(15), 8976–8984.
617 https://doi.org/10.1029/2019GL083701

618 Florin, M.-V. (2021). Combatting climate change through a portfolio of approaches. Spotlight on Risk, 1.
619 https://www.epfl.ch/research/domains/irgc/combatting-climate-change-through-a-portfolio-of-approaches/

620 Frich, P., Alexander, L. V., Della-Marta, P., Gleason, B., Haylock, M., Klein Tank, A. M. G., & Peterson, T.
621 (2002). Observed coherent changes in climatic extremes during the second half of the twentieth century.
622 Climate Research, 19(3), 193–212. https://doi.org/10.3354/cr019193

623 Gabriel, C. J., & Robock, A. (2015). Stratospheric geoengineering impacts on El Niño/Southern Oscillation.
624 Atmospheric Chemistry and Physics, 15(20), 11949–11966. https://doi.org/10.5194/acp-15-11949-2015

625 Gertler, C. G., O'Gorman, P. A., Kravitz, B., Moore, J. C., Phipps, S. J., & Watanabe, S. (2020). Weakening of
626 the Extratropical Storm Tracks in Solar Geoengineering Scenarios. Geophysical Research Letters, 47(11).
627 https://doi.org/10.1029/2020GL087348

628 Giorgi, F., Coppola, E., & Raffaele, F. (2014). A consistent picture of the hydroclimatic response to global
629 warming from multiple indices: Models and observations: hydroclimatic response to global warming.
630 Journal of Geophysical Research: Atmospheres, 119(20), 11,695-11,708.
631 https://doi.org/10.1002/2014JD022238

https://doi.org/10.5194/egusphere-2022-1
Preprint. Discussion started: 14 March 2022

632 Giorgi, F., Raffaele, F., & Coppola, E. (2019). The response of precipitation characteristics to global warming
633 from climate projections. Earth System Dynamics, 10(1), 73–89. https://doi.org/10.5194/esd-10-73-2019

634 Guerreiro, S. B., Fowler, H. J., Barbero, R., Westra, S., Lenderink, G., Blenkinsop, S., Lewis, E., & Li, X.-F.
635 (2018). Detection of continental-scale intensification of hourly rainfall extremes. Nature Climate Change,
636 8(9), 803–807. https://doi.org/10.1038/s41558-018-0245-3

637 Halladay, K., & Good, P. (2017). Non-linear interactions between CO 2 radiative and physiological effects on
638 Amazonian evapotranspiration in an Earth system model. Climate Dynamics, 49(7–8), 2471–2490.
639 https://doi.org/10.1007/s00382-016-3449-0

640 Haywood, J. M., Jones, A., Bellouin, N., & Stephenson, D. (2013). Asymmetric forcing from stratospheric
641 aerosols impacts Sahelian rainfall. Nature Climate Change, 3(7), 660–665.
642 https://doi.org/10.1038/nclimate1857

643 Honegger, M., Burns, W., & Morrow, D. R. (2021). Is carbon dioxide removal 'mitigation of climate change'?
644 Review of European, Comparative & International Environmental Law, 30(3), 327–335.
645 https://doi.org/10.1111/reel.12401

646 Ingram, W. (2016). Increases all round. Nature Climate Change, 6(5). https://doi.org/doi:10.1038/nclimate2966

647 Irvine, P., Emanuel, K., He, J., Horowitz, L. W., Vecchi, G., & Keith, D. (2019). Halving warming with idealized
648 solar geoengineering moderates key climate hazards. Nature Climate Change, 9(4), 295–299.
649 https://doi.org/10.1038/s41558-019-0398-8

650 Ji, D., Fang, S., Curry, C. L., Kashimura, H., Watanabe, S., Cole, J. N. S., Lenton, A., Muri, H., Kravitz, B., &
651 Moore, J. C. (2018). Extreme temperature and precipitation response to solar dimming and stratospheric
652 aerosol geoengineering. Atmospheric Chemistry and Physics, 18(14), 10133–10156.
653 https://doi.org/10.5194/acp-18-10133-2018

654 Jiang, J., Cao, L., MacMartin, D. G., Simpson, I. R., Kravitz, B., Cheng, W., Visioni, D., Tilmes, S., Richter, J.
655 H., & Mills, M. J. (2019). Stratospheric Sulfate Aerosol Geoengineering Could Alter the High-Latitude
656 Seasonal Cycle. Geophysical Research Letters, 46(23), 14153–14163.
657 https://doi.org/10.1029/2019GL085758

https://doi.org/10.5194/egusphere-2022-1
Preprint. Discussion started: 14 March 2022

658 Jones, A. C., Hawcroft, M. K., Haywood, J. M., Jones, A., Guo, X., & Moore, J. C. (2018). Regional Climate
659 Impacts of Stabilizing Global Warming at 1.5 K Using Solar Geoengineering. Earth's Future, 6(2), 230–
660 251. https://doi.org/10.1002/2017EF000720

661 Karami, K., Tilmes, S., Muri, H., & Mousavi, S. V. (2020). Storm Track Changes in the Middle East and North
662 Africa Under Stratospheric Aerosol Geoengineering. Geophysical Research Letters, 47(14).
663 https://doi.org/10.1029/2020GL086954

664 Keith, D. W., & Irvine, P. J. (2016). Solar geoengineering could substantially reduce climate risks-A research
665 hypothesis for the next decade. Earth's Future, 4(11), 549–559. https://doi.org/10.1002/2016EF000465

666 Kharin, V. V., Flato, G. M., Zhang, X., Gillett, N. P., Zwiers, F., & Anderson, K. J. (2018). Risks from Climate
667 Extremes Change Differently from 1.5°C to 2.0°C Depending on Rarity. Earth's Future, 6(5), 704–715.
668 https://doi.org/10.1002/2018EF000813

669 Kim, Y.-H., Min, S.-K., Zhang, X., Sillmann, J., & Sandstad, M. (2020). Evaluation of the CMIP6 multi-model
670 ensemble for climate extreme indices. Weather and Climate Extremes, 29, 100269.
671 https://doi.org/10.1016/j.wace.2020.100269

672 Klein-Tank, A. M. G., Zwiers, F. W., & Zhang, X. (2009). Guidelines on Analysis of extremes in a changing
673 climate in support of informed decisions for adaptation. In Climate Data and Monitoring (WCDMP-No. 72;
674 p. 52). World Meteorological Organization. File Attachment

675 Kravitz, B., MacMartin, D. G., Mills, M. J., Richter, J. H., Tilmes, S., Lamarque, J., Tribbia, J. J., & Vitt, F.
676 (2017). First Simulations of Designing Stratospheric Sulfate Aerosol Geoengineering to Meet Multiple
677 Simultaneous Climate Objectives. Journal of Geophysical Research: Atmospheres, 122(23).
678 https://doi.org/10.1002/2017JD026874

679 Kravitz, B., MacMartin, D. G., Tilmes, S., Richter, J. H., Mills, M. J., Cheng, W., Dagon, K., Glanville, A. S.,
680 Lamarque, J., Simpson, I. R., Tribbia, J., & Vitt, F. (2019). Comparing Surface and Stratospheric Impacts
681 of Geoengineering With Different SO2 Injection Strategies. Journal of Geophysical Research: Atmospheres,
682 124(14), 7900–7918. https://doi.org/10.1029/2019JD030329

683 Kravitz, B., MacMartin, D. G., Visioni, D., Boucher, O., Cole, J. N. S., Haywood, J., Jones, A., Lurton, T., Nabat,
684 P., Niemeier, U., Robock, A., Séférian, R., & Tilmes, S. (2021). Comparing different generations of idealized

https://doi.org/10.5194/egusphere-2022-1
Preprint. Discussion started: 14 March 2022

685 solar geoengineering simulations in the Geoengineering Model Intercomparison Project (GeoMIP).
686 Atmospheric Chemistry and Physics, 21(6), 4231–4247. https://doi.org/10.5194/acp-21-4231-2021

687 Kravitz, B., MacMartin, D. G., Wang, H., & Rasch, P. J. (2016). Geoengineering as a design problem. Earth
688 System Dynamics. https://doi.org/10.5194/esd-7-469-2016

689 Kravitz, B., Robock, A., Boucher, O., Schmidt, H., Taylor, K. E., Stenchikov, G., & Schulz, M. (2011). The
690 Geoengineering Model Intercomparison Project (GeoMIP). Atmospheric Science Letters, 12(2), 162–167.
691 https://doi.org/10.1002/asl.316

692 Krishnamohan, K. S., & Bala, G. (2022). Sensitivity of tropical monsoon precipitation to the latitude of
693 stratospheric aerosol injections. Climate Dynamics. https://doi.org/10.1007/s00382-021-06121-z

694 Kuswanto, H., Kravitz, B., Miftahurrohmah, B., Fauzi, F., Sopahaluwaken, A., & Moore, J. (2021). Impact of
695 solar geoengineering on temperatures over the Indonesian Maritime Continent. International Journal of
696 Climatology, joc.7391. https://doi.org/10.1002/joc.7391

697 Lee, W., MacMartin, D., Visioni, D., & Kravitz, B. (2020). Expanding the design space of stratospheric aerosol
698 geoengineering to include precipitation-based objectives and explore trade-offs. Earth System Dynamics,
699 11(4), 1051–1072. https://doi.org/10.5194/esd-11-1051-2020

700 Logan, J. A., Macfarlane, W. W., & Willcox, L. (2010). Whitebark pine vulnerability to climate-driven mountain
701 pine beetle disturbance in the Greater Yellowstone Ecosystem. Ecological Applications, 20, 895–902.
702 https://doi.org/10.1890/09-0655.1

703 MacMartin, D. G., Keith, D. W., Kravitz, B., & Caldeira, K. (2013). Management of trade-offs in geoengineering
704 through optimal choice of non-uniform radiative forcing. Nature Climate Change, 3(4), 365–368.
705 https://doi.org/10.1038/nclimate1722

706 MacMartin, D. G., Kravitz, B., Tilmes, S., Richter, J. H., Mills, M. J., Lamarque, J. F., Tribbia, J. J., & Vitt, F.
707 (2017). The Climate Response to Stratospheric Aerosol Geoengineering Can Be Tailored Using Multiple
708 Injection Locations. Journal of Geophysical Research: Atmospheres, 122(23).
709 https://doi.org/10.1002/2017JD026868

710 MacMartin, D. G., Ricke, K. L., & Keith, D. W. (2018). Solar geoengineering as part of an overall strategy for
711 meeting the 1.5°C Paris target. Philosophical Transactions of the Royal Society A: Mathematical, Physical
712 and Engineering Sciences, 376(2119), 20160454. https://doi.org/10.1098/rsta.2016.0454

https://doi.org/10.5194/egusphere-2022-1
Preprint. Discussion started: 14 March 2022

Malik, A., Nowack, P. J., Haigh, J. D., Cao, L., Atique, L., & Plancherel, Y. (2020). Tropical Pacific climate variability under solar geoengineering: Impacts on ENSO extremes. Atmospheric Chemistry and Physics, 20(23), 15461–15485. https://doi.org/10.5194/acp-20-15461-2020

Mearns, L. O., Katz, R. W., & Schneider, S. H. (1984). Extreme High-Temperature Events: Changes in their probabilities with Changes in Mean Temperature. Journal of Climate and Applied Meteorology, 23(12), 1601–1613. https://doi.org/10.1175/1520-0450(1984)023<1601:EHTECI>2.0.CO;2

Meehl, G. A., Zwiers, F., Evans, J., Knutson, T., Mearns, L., & Whetton, P. (2000). Trends in Extreme Weather and Climate Events: Issues Related to Modeling Extremes in Projections of Future Climate Change *. Bulletin of the American Meteorological Society, 81(3), 427–436. https://doi.org/10.1175/1520-0477(2000)081<0427:TIEWAC>2.3.CO;2

Mills, J. N., Gage L., K., & Khan, A. (2010). Potential influence of climate change on vector-borne and zoonotic diseases: A review and proposed research plan. Environ. Health Perspect., 118, 1507–1514. https://doi.org/10.1289/ehp.0901389

Mitchell, D., Heaviside, C., Vardoulakis, S., Huntingford, C., Masato, G., P Guillod, B., Frumhoff, P., Bowery, A., Wallom, D., & Allen, M. (2016). Attributing human mortality during extreme heat waves to anthropogenic climate change. Environmental Research Letters, 11(7), 074006. https://doi.org/10.1088/1748-9326/11/7/074006

Muthyala, R., Bala, G., & Nalam, A. (2018a). Regional scale analysis of climate extremes in an SRM geoengineering simulation, Part 1: Precipitation extremes. Current Science, 114(5), 1024.

Muthyala, R., Bala, G., & Nalam, A. (2018b). Regional scale analysis of climate extremes in an SRM geoengineering simulation, Part 2: Temperature extremes. Current Science, 114(5), 1036.

Odoulami, R. C., New, M., Wolski, P., Guillemet, G., Pinto, I., Lennard, C., Muri, H., & Tilmes, S. (2020). Stratospheric Aerosol Geoengineering could lower future risk of 'Day Zero' level droughts in Cape Town. Environmental Research Letters, 15(12), 124007. https://doi.org/10.1088/1748-9326/abbf13

Oleson, K., Lawrence, D., Bonan, G., Drewniak, B., Huang, M., Koven, C., Levis, S., Li, F., Riley, W., Subin, Z., Swenson, S., Thornton, P., Bozbiyik, A., Fisher, R., Heald, C., Kluzek, E., Lamarque, J.-F., Lawrence, P., Leung, L., … Yang, Z.-L. (2013). Technical description of version 4.5 of the Community Land Model (CLM) (p. 5912 KB) UCAR/NCAR. https://doi.org/10.5065/D6RR1W7M

https://doi.org/10.5194/egusphere-2022-1
Preprint. Discussion started: 14 March 2022

741 Pendergrass, A. G., & Knutti, R. (2018). The Uneven Nature of Daily Precipitation and Its Change. Geophysical
742 Research Letters, 45(21), 11,980-11,988. https://doi.org/10.1029/2018GL080298

743 Pinto, I., Jack, C., Lennard, C., Tilmes, S., & Odoulami, R. C. (2020). Africa's Climate Response to Solar
744 Radiation Management With Stratospheric Aerosol. Geophysical Research Letters.
745 https://doi.org/10.1029/2019GL086047

746 Seltenrich, N. (2015). Between Extremes: Health Effects of Heat and Cold. Environmental Health Perspectives,
747 123(11). https://doi.org/10.1289/ehp.123-A275

748 Seneviratne, S. I., Zhang, X., Adnan, M., Badi, W., Dereczynski, C., Di Luca, A., Ghosh, S., Iskandar, I., Kossin,
749 J. P., Lewis, S. C., Otto, F. E. L., Pinto, I., Satoh, M., Vicente-Serrano, S. M., Wehner, M., & Zhou, B.
750 (2021). Weather and Climate Extremes in a Changing Climate. In V. Masson-Delmotte, P. Zhai, A. Pirani,
751 S. L. Connors, C. Péan, S. Berger, N. Caud, Y. Chen, L. Goldfarb, M. I. Gomis, M. Huang, K. Leitzell, E.
752 Lonnoy, J. B. R. Matthews, T. K. Maycock, T. Waterfield, O. Yeleçki, R. Yu, & B. Zhou (Eds.), Climate
753 Change 2021: The Physical Science Basis. Contribution of Working Group I to the Sixth Assessment Report
754 of the Intergovernmental Panel on Climate Change. Cambridge University Press.

755 Sillmann, J., Kharin, V. V., Zhang, X., Zwiers, F. W., & Bronaugh, D. (2013a). Climate extremes indices in the
756 CMIP5 multimodel ensemble: Part 1. Model evaluation in the present climate. Journal of Geophysical
757 Research: Atmospheres, 118(4), 1716–1733. https://doi.org/10.1002/jgrd.50203

758 Sillmann, J., Kharin, V. V., Zwiers, F. W., Zhang, X., & Bronaugh, D. (2013b). Climate extremes indices in the
759 CMIP5 multimodel ensemble: Part 2. Future climate projections. Journal of Geophysical Research:
760 Atmospheres, 118(6), 2473–2493. https://doi.org/10.1002/jgrd.50188

761 Simpson, I. R., Tilmes, S., Richter, J. H., Kravitz, B., MacMartin, D. G., Mills, M. J., Fasullo, J. T., & Pendergrass,
762 A. G. (2019). The Regional Hydroclimate Response to Stratospheric Sulfate Geoengineering and the Role
763 of Stratospheric Heating. Journal of Geophysical Research: Atmospheres, 124(23), 12587–12616.
764 https://doi.org/10.1029/2019JD031093

765 Smith, K. R., Woodward, A., Campbell-Lundrum, D., Chadee, D. D., Honda, Y., Liu, Q., Olwoch, J. M., Revich,
766 B., & Sauerborn, R. (2014). 2014: Human health: Impacts, adaptation, and co-benefits. In C. B. Field, V. R.
767 Barros, D. J. Dokken, K. J. Mach, M. D. Mastrandrea, T. E. Bilir, M. Chatterjee, K. L. Ebi, Y. O. Estrada,
768 R. C. Genova, B. Girma, E. S. Kissel, A. N. Levy, S. MacCracken, P. R. Mastrandrea, & L. L. White (Eds.),
769 Climate Change 2014: Impacts, Adaptation, and Vulnerability. Part A: Global and Sectoral Aspects.

https://doi.org/10.5194/egusphere-2022-1
Preprint. Discussion started: 14 March 2022

Contribution of Working Group II to the Fifth Assessment Report of the Intergovernmental Panel on Climate Change (pp. 709–754). Cambridge University Press.

Stott, P. (2016). How climate change affects extreme weather events. Science, 352(6293), 1517–1518. https://doi.org/10.1126/science.aaf7271

Tebaldi, C., Dorheim, K., Wehner, M., & Leung, R. (2021). Extreme metrics from large ensembles: Investigating the effects of ensemble size on their estimates. Earth System Dynamics, 12(4), 1427–1501. https://doi.org/10.5194/esd-12-1427-2021

Tebaldi, C., & Wehner, M. F. (2018). Benefits of mitigation for future heat extremes under RCP4.5 compared to RCP8.5. Climatic Change, 146(3–4), 349–361. https://doi.org/10.1007/s10584-016-1605-5

Tilmes, S., MacMartin, D. G., Lenaerts, J. T. M., van Kampenhout, L., Muntjewerf, L., Xia, L., Harrison, C. S., Krumhardt, K. M., Mills, M. J., Kravitz, B., & Robock, A. (2020). Reaching 1.5 and 2.0 °C global surface temperature targets using stratospheric aerosol geoengineering. Earth System Dynamics, 11(3), 579–601. https://doi.org/10.5194/esd-11-579-2020

Tilmes, S., Richter, J. H., Kravitz, B., MacMartin, D. G., Mills, M. J., Simpson, I. R., Glanville, A. S., Fasullo, J. T., Phillips, A. S., Lamarque, J.-F., Tribbia, J., Edwards, J., Mickelson, S., & Ghosh, S. (2018). CESM1(WACCM) Stratospheric Aerosol Geoengineering Large Ensemble Project. Bulletin of the American Meteorological Society, 99(11), 2361–2371. https://doi.org/10.1175/BAMS-D-17-0267.1

Trisos, C. H., Amatulli, G., Gurevitch, J., Robock, A., Xia, L., & Zambri, B. (2018). Potentially dangerous consequences for biodiversity of solar geoengineering implementation and termination. Nature Ecology & Evolution, 2(3), 475–482. https://doi.org/10.1038/s41559-017-0431-0

Tye, M. R., Blenkinsop, S., Bosilovich, M. G., Donat, M. G., Durre, I., Simmons, A. J., & Ziese, M. (2021). Land Surface Precipitation Extremes [in "State of the Climate in 2020"]. Bulletin of the American Meteorological Society.

Visioni, D., MacMartin, D. G., & Kravitz, B. (2021). Is Turning Down the Sun a Good Proxy for Stratospheric Sulfate Geoengineering? Journal of Geophysical Research: Atmospheres, 126(5). https://doi.org/10.1029/2020JD033952

https://doi.org/10.5194/egusphere-2022-1
Preprint. Discussion started: 14 March 2022

796 Visioni, D., MacMartin, D. G., Kravitz, B., Richter, J. H., Tilmes, S., & Mills, M. J. (2020). Seasonally Modulated
797 Stratospheric Aerosol Geoengineering Alters the Climate Outcomes. Geophysical Research Letters, 47(12).
798 https://doi.org/10.1029/2020GL088337

799 Wei, L., Ji, D., Miao, C., Muri, H., & Moore, J. C. (2018). Global streamflow and flood response to stratospheric
800 aerosol geoengineering. Atmospheric Chemistry and Physics, 18(21), 16033–16050.
801 https://doi.org/10.5194/acp-18-16033-2018

802 Xia, L., Robock, A., Tilmes, S., & Neely III, R. R. (2016). Stratospheric sulfate geoengineering could enhance
803 the terrestrial photosynthesis rate. Atmospheric Chemistry and Physics, 16(3), 1479–1489.
804 https://doi.org/10.5194/acp-16-1479-2016

805 Zarnetske, P. L., Gurevitch, J., Franklin, J., Groffman, P. M., Harrison, C. S., Hellmann, J. J., Hoffman, F. M.,
806 Kothari, S., Robock, A., Tilmes, S., Visioni, D., Wu, J., Xia, L., & Yang, C.-E. (2021). Potential ecological
807 impacts of climate intervention by reflecting sunlight to cool Earth. Proceedings of the National Academy
808 of Sciences, 118(15), e1921854118. https://doi.org/10.1073/pnas.1921854118

809 Zhang, X., Alexander, L., Hegerl, G. C., Jones, P., Tank, A. K., Peterson, T. C., Trewin, B., & Zwiers, F. W.
810 (2011). Indices for monitoring changes in extremes based on daily temperature and precipitation data. Wiley
811 Interdisciplinary Reviews: Climate Change, 2, 851–870. https://doi.org/10.1002/wcc.147

812

813

https://doi.org/10.5194/egusphere-2022-1
Preprint. Discussion started: 14 March 2022

814 **Table Captions**

815 Table 1: Summary of simulations carried out as part of the GLENS project: simulation name, ensemble
816 members, simulation time period, and analysis period.

817

818 Table 2: Selection of extreme indices developed by ETCCDI (Klein Tank et al., 2009) _Percentiles marked with
819 * were estimated from a base period of 2010-2030 but are not included in the main text; values are calculated as
820 a climatological average for the end of the century (2075-2095). Indices in italics are not included in the main
821 text.

822

823

824

https://doi.org/10.5194/egusphere-2022-1
Preprint. Discussion started: 14 March 2022

Figure Captions

Figure 1: AR6 Reference Regions for Land (Source: Iturbide et al., 2020)

Figure 2: Projected anomalies between the GLENS EC scenario (2075-2095) and BASE (2010-2030) for annual coldest night and day (TNn, TXn), and warmest night and day (TNx, TXx) shown in the left column, and for anomalies between RCP8.5 EC (2075-2095) and BASE (2010-2030) shown in the right column. Note that the colorbar is different in the right column. Hatching indicates significance at the 5% test level using the Student's t-test.

Figure 3: Climatological mean of coldest night (TNn) for: BASE (2010-2030) in grey, GLENS End of Century (EC; 2075-2095) in blue and RCP8.5 EC in red in each of the AR6 regions except Antarctica (Iturbide et al., 2019). Boxes show ensemble mean in white with the limits set at 25% and 75% of the ensemble spread; whiskers denote 5% and 95% ensemble spread.

Figure 4: The same as Figure 2, but containing projected anomalies in the frequency of daily minima <0°C (frost days, FD), daily maxima <0°C (ice days, ID), daily minima >20°C (tropical nights, TR) and daily maxima >25°C (summer days, SU). Hatching indicates significance at the 5% test level using the Student's t-test.

Figure 5: Ensemble mean of projected changes in mean global temperature for GLENS EC (2075-2095) minus BASE (2010-2030) with inset regional time series of the warmest night (TNx) for Northeast North America (NEN), North Central America (NCA), Sahara (SAH), North Europe (NEU), Arabian Peninsula (ARP), South Asia (SAS), East Asia (EAS) and East Australia (EAU).

Figure 6: Similar to Figure 2, but for projected changes in a) annual precipitation (PRCPTOT), b) the mean wet day volume (SDII), c) annual maximum precipitation (Rx1day), and d) annual wettest pentad (Rx5day). Hatching indicates significance at the 5% test level using the Student's t-test.

Figure 7: Similar to Figure 2, but for projected changes in a) the longest spell of dry days (CDD) and b) longest spell of wet days (CWD). Hatching indicates significance at the 5% test level using the Student's t-test.

Figure 8: Similar to Figure 2, but for projected changes in a) the frequency of days with heavy precipitation (R10mm) and b) days with very heavy precipitation (R20mm). Hatching indicates significance at the 5% test level using the Student's t-test.

Figure 9: Ensemble mean of projected changes in mean daily precipitation for GLENS EC (2075-2095) minus BASE (2010-2030) with inset regional time series of frequency of days >10mm (R10mm) for Northeast North

https://doi.org/10.5194/egusphere-2022-1
Preprint. Discussion started: 14 March 2022

America (NEN), North South America (NSA), South Eastern Africa (SES), Western Africa (WAF), Eastern Europe (EEU), South Asia (SAS), East Asia (EAS) and North Australia (NAU).

Figure 10: Projected changes between GLENS EC (2075-2095) and BASE (2010-2030) in a) latent heat flux; b) soil moisture in the top 10cm; c) total leaf area index; and d) gross primary production. Black polygons highlight the following regions: Northeast South America (NSA), North South America, Western Africa (WAF), Central Africa (CAF), and South Asia (SAS).

Figure 11: Projected changes between GLENS EC (2075-2095) and BASE (2010-2030) in a) ground evaporation, b) canopy evaporation, and c) transpiration. Highlighted regions as for Figure 10.